

1 Global maps of soil temperature

2 *Running head: Global maps of soil temperature*

3

4 Jonas J. Lembrechts^{1,*^x}, Johan van den Hoogen^{2,*}, Juha Aalto^{3,4}, Michael B. Ashcroft^{5,6}, Pieter De Frenne⁷, Julia
5 Kemppinen⁸, Martin Kopecký^{9,10}, Miska Luoto⁴, Ilya M. D. Maclean¹¹, Thomas W. Crowther², Joseph J. Bailey¹²,
6 Stef Haesen¹³, David H. Klings^{14,15}, Pekka Niittynen⁴, Brett R. Scheffers¹⁶, Koenraad Van Meerbeek¹³, Peter
7 Aartsma¹⁷, Otar Abdalaze¹⁸, Mehdi Abedi¹⁹, Rien Aerts²⁰, Negar Ahmadian¹⁹, Antje Ahrends²¹, Juha M. Alatalo²²,
8 Jake M. Alexander²³, Camille Nina Allonsius²⁴, Jan Altman⁹, Christof Ammann²⁵, Christian Andres²⁶, Christopher
9 Andrews²⁷, Jonas Ardö²⁸, Nicola Arriga²⁹, Alberto Arzac³⁰, Valeria Ascherö^{31,32}, Rafael L. Assis³³, Jakob Johann
10 Assmann^{34,35}, Maaike Y. Bader³⁶, Khadijeh Bahalkeh¹⁹, Peter Barančok³⁷, Isabel C. Barrio³⁸, Agustina Barros³⁹,
11 Matti Barthel²⁶, Edmund W. Basham¹⁴, Marijn Bauters⁴⁰, Manuele Bazzichetto⁴¹, Luca Belelli Marchesini⁴²,
12 Michael C. Bell⁴³, Juan C. Benavides⁴⁴, José Luis Benito Alonso⁴⁵, Bernd J. Berauer^{46,47}, Jarle W. Bjerke⁴⁸, Robert
13 G. Björk^{49,50}, Mats P. Björkman^{49,50}, Katrin Björnsdóttir⁵¹, Benjamin Blonder⁵², Pascal Boeckx⁴⁰, Julia Boike^{53,54},
14 Stef Bokhorst²⁰, Bárbara N. S. Brum⁵⁵, Josef Brůna⁹, Nina Buchmann²⁶, Pauline Buysse⁵⁶, José Luís Camargo⁵⁷,
15 Otávio C. Campoe⁵⁸, Onur Candan⁵⁹, Rafaella Canessa^{60,61}, Nicoletta Cannone⁶², Michele Carbognani⁶³, Jofre
16 Carnicer^{64,65}, Angélica Casanova-Katny⁶⁶, Simone Cesarz^{67,68}, Bogdan Chojnicki^{69,69}, Philippe Choler^{70,71}, Steven L.
17 Chown⁷², Edgar F. Cifuentes⁷³, Marek Čiliak⁷⁴, Tamara Contador^{75,76}, Peter Convey⁷⁷, Elisabeth J. Cooper⁷⁸,
18 Edoardo Cremonese⁷⁹, Salvatore R. Curasi⁸⁰, Robin Curtis¹¹, Maurizio Cutini⁸¹, C. Johan Dahlberg^{82,83}, Gergana N.
19 Daskalova⁸⁴, Miguel Angel de Pablo⁸⁵, Stefano Della Chiesa⁸⁶, Jürgen Dengler^{87,88,67}, Bart Deronde⁸⁹, Patrice
20 Descombes⁹⁰, Valter Di Cecco⁹¹, Michele Di Musciano⁹², Jan Dick²⁷, Romina D. Dimarco^{93,94}, Jiri Dolezal^{9,95}, Ellen
21 Dorrepaal⁹⁶, Jiří Dušek⁹⁷, Nico Eisenhauer^{67,68}, Lars Eklundh²⁸, Brian Enquist⁹⁸, Todd E. Erickson^{99,100}, Brigitta
22 Erschbamer¹⁰¹, Werner Eugster²⁶, Robert M. Ewers¹⁰², Dan A. Exton¹⁰³, Nicolas Fanin¹⁰⁴, Fatih Fazlioglu⁵⁹, Iris
23 Feigenwinter²⁶, Giuseppe Fenu¹⁰⁵, Olga Ferlian^{67,68}, M. Rosa Fernández Calzado¹⁰⁶, Eduardo Fernández-
24 Pascual¹⁰⁷, Manfred Finckh¹⁰⁸, Rebecca Finger Higgens¹⁰⁹, T'ai G. W. Forte⁶³, Erika C. Freeman¹¹⁰, Esther R.
25 Frei^{111,112}, Eduardo Fuentes-Lillo^{113,1,114}, Rafael A. García^{113,115}, María B. García¹¹⁶, Charly Géron¹¹⁷, Mana
26 Gharun²⁶, Dany Ghosn¹¹⁸, Khatuna Gigauri¹¹⁹, Anne Gobin^{120,121}, Ignacio Goded²⁹, Mathias Goeckede¹²², Felix
27 Gottschall^{67,68}, Keith Goulding¹²³, Sanne Govaert⁷, Bente Jessen Graae¹²⁴, Sarah Greenwood¹²⁵, Caroline
28 Greiser⁸², Achim Grelle¹²⁶, Benoit Guénard¹²⁷, Mauro Guglielmin¹²⁸, Joannès Guillemot^{129,130}, Peter Haase^{131,132},
29 Sylvia Haider^{133,67}, Aud H. Halbritter¹³⁴, Maroof Hamid¹³⁵, Albin Hammerle¹³⁶, Arndt Hampe¹³⁷, Siri V.
30 Haugum^{134,138}, Lucia Hederová⁹, Bernard Heinesch¹³⁹, Carole Helfter¹⁴⁰, Daniel Hepenstrick⁸⁷, Maximiliane
31 Herberich¹⁴¹, Mathias Herbst¹⁴², Luise Hermanutz¹⁴³, David S. Hik¹⁴⁴, Raúl Hoffré¹⁴⁵, Jürgen Homeier¹⁴⁶, Lukas
32 Hörtnagl²⁶, Toke T. Høye¹⁴⁷, Filip Hrbacek¹⁴⁸, Kristoffer Hylander⁸², Hiroki Iwata¹⁴⁹, Marcin Antoni Jackowicz-
33 Korczynski^{150,28}, Hervé Jactel¹⁵¹, Järvi Järveoja¹⁵², Janusz Olejnik¹⁵³, Szymon Jastrzębowski¹⁵⁴, Anke Jentsch^{47,155},
34 Juan J. Jiménez¹⁵⁶, Ingibjörg S. Jónsdóttir¹⁵⁷, José João L. L. Souza¹⁵⁸, Tommaso Jucker¹⁵⁹, Alistair S. Jump¹⁶⁰,
35 Radoslaw Juszczak⁶⁹, Róbert Kanka³⁷, Vít Kašpar^{9,161}, George Kazakis¹¹⁸, Julia Kelly¹⁶², Anzar A. Khuroo¹³⁵, Leif
36 Klemetsson⁴⁹, Marcin Klisz¹⁵⁴, Natascha Kljun¹⁶², Alexander Knohl¹⁶³, Johannes Kobler¹⁶⁴, Jozef Kollár³⁷, Olaf
37 Kolle¹⁶⁵, Martyna M. Kotowska¹⁴⁶, Bence Kovács¹⁶⁶, Juergen Kreyling¹⁶⁷, Andrea Lamprecht¹⁶⁸, Simone I. Lang¹⁶⁹,
38 Christian Larson¹⁷⁰, Keith Larson¹⁷¹, Kamil Laska^{148,172}, Guerric le Maire^{129,130}, Rachel I. Leihy¹⁷³, Luc Lens¹⁷⁴, Bengt
39 Liljebladh⁴⁹, Annalea Lohila^{175,176}, Juan Lorite^{106,177}, Benjamin Loubet⁵⁶, Joshua Lynn¹³⁴, Martin Macek⁹, Roy
40 Mackenzie⁷⁵, Enzo Magliulo¹⁷⁸, Regine Maier²⁶, Francesco Malfasi⁶², František Máliš¹⁷⁹, Matěj Man⁹, Giovanni
41 Manca²⁹, Antonio Manco¹⁸⁰, Tanguy Manise¹³⁹, Paraskevi Manolaki^{181,182,183}, Felipe Marciňiak⁵⁵, Marianna
42 Nardino¹⁸⁴, Radim Matula^{10,185}, Ana Clara Mazzolari³², Sergiy Medinets^{186,187,188}, Volodymyr Medinets¹⁸⁶, Camille
43 Meeussen⁷, Sonia Merinero⁸², Rita de Cássia Guimarães Mesquita¹⁸⁹, Katrin Meusburger¹⁹⁰, Filip J. R.
44 Meysman¹⁹¹, Sean T. Michaletz¹⁹², Ann Milbau¹⁹³, Dmitry Moiseev¹⁹⁴, Pavel Moiseev¹⁹⁴, Andrea Mondoni¹⁹⁵, Ruth
45 Monfries²¹, Leonardo Montagnani¹⁹⁶, Mikel Moriana-Armendariz⁷⁸, Umberto Morra di Cella¹⁹⁷, Martin
46 Mörsdorf¹⁹⁸, Jonathan R. Mosedale¹⁹⁹, Lena Muffler¹⁴⁶, Miriam Muñoz-Rojas^{200,99}, Jonathan A. Myers²⁰¹, Isla H.

47 Myers-Smith⁸⁴, Laszlo Nagy²⁰², Ilona Naujokaitis-Lewis²⁰³, Emily Newling²⁰⁴, Lena Nicklas¹⁰¹, Georg Niedrist²⁰⁵,
48 Armin Niessner²⁰⁶, Mats B. Nilsson¹⁵², Signe Normand^{34,35}, Marcelo D. Nosetto^{207,208}, Yann Nouvellon^{129,130},
49 Martin A. Nuñez^{209,94}, Romà Ogaya^{210,211}, Jérôme Ogée¹⁰⁴, Joseph Okello^{40,212,213}, Jørgen Eivind Olesen²¹⁴, Øystein
50 Opedal²¹⁵, Simone Orsenigo²¹⁶, Andrej Palaj³⁷, Timo Pampuch²¹⁷, Alexey V. Panov²¹⁸, Meelis Pärtel²¹⁹, Ada
51 Pastor^{220,182}, Aníbal Pauchard^{113,115}, Harald Pauli¹⁶⁸, Marian Pavelka⁹⁷, William D. Pearse^{221,222}, Matthias Peichl¹⁵²,
52 Loïc Pellissier^{223,224}, Rachel M. Penczykowski²²⁵, Josep Penuelas^{210,211}, Matteo Petit Bon^{169,78,9}, Alessandro
53 Petraglia⁶³, Shyam S. Phartyal²²⁶, Gareth K. Phoenix²²⁷, Casimiro Pio²²⁸, Andrea Pitacco²²⁹, Camille Pitteloud^{223,224},
54 Roman Plichta¹⁸⁵, Francesco Porro¹⁹⁵, Miguel Portillo-Estrada¹, Jérôme Poulenard²³⁰, Rafael Poyatos^{65,231},
55 Anatoly S. Prokushkin^{218,30}, Radoslaw Puchalka^{232,233}, Mihai Pușcaș^{234,235,236}, Dajana Radujković¹, Krystal
56 Randall^{5,237}, Amanda Ratier Backes^{133,67}, Sabine Remmelle²⁰⁶, Wolfram Remmers²³⁸, David Renault^{41,239}, Anita C.
57 Risch²⁴⁰, Christian Rixen¹¹¹, Sharon A. Robinson^{5,237}, Bjorn J.M. Robroek²⁴², Adrian V. Rocha²⁴³, Christian
58 Rossi^{244,245}, Graziano Rossi¹⁹⁵, Olivier Rouspard^{246,247,248}, Alexey V. Rubtsov³⁰, Patrick Saccone¹⁶⁸, Clotilde Sagot²⁴⁹,
59 Jhonatan Sallo Bravo^{250,251}, Cinthya C. Santos²⁵², Judith M. Sarneel²⁵³, Tobias Scharnweber²¹⁷, Jonas
60 Schmeddes¹⁶⁷, Marius Schmidt²⁵⁴, Thomas Scholten²⁵⁵, Max Schuchardt⁴⁷, Naomi Schwartz²⁵⁶, Tony Scott¹²³, Julia
61 Seeber^{205,257}, Ana Cristina Segalin de Andrade²⁵², Tim Seipe¹⁷⁰, Philipp Semenchuk²⁵⁸, Rebecca A. Senior²⁵⁹, Josep
62 M. Serra-Diaz²⁶⁰, Piotr Sewerniak²⁶¹, Ankit Shekhar²⁶, Nikita V. Sidenko²¹⁸, Lukas Siebické¹⁶³, Laura Siegwart
63 Collier^{143,262}, Elizabeth Simpson²²¹, David P. Siqueira²⁶³, Zuzana Sitková²⁶⁴, Johan Six²⁶, Marko Smiljanic²¹⁷, Stuart
64 W. Smith^{124,265}, Sarah Smith-Tripp²⁶⁶, Ben Somers²⁶⁷, Mia Vedel Sørensen¹²⁴, Bartolomeu Israel Souza²⁶⁸, Arildo
65 Souza Dias^{269,252}, Marko J. Spasojevic²⁷⁰, James D. M. Speed²⁷¹, Fabien Spicher²⁷², Angela Stanisci²⁷³, Klaus
66 Steinbauer¹⁶⁸, Rainer Steinbrecher²⁷⁴, Michael Steinwandter²⁰⁵, Michael Stemkovski²²¹, Jörg G. Stephan²⁷⁵,
67 Christian Stiegler¹⁶³, Stefan Stoll^{238,276}, Martin Svátek¹⁸⁵, Miroslav Svoboda¹⁰, Torben Tagesson^{28,277}, Andrew J.
68 Tanentzap¹¹⁰, Franziska Tanneberger²⁷⁸, Jean-Paul Theurillat^{279,280}, Haydn J. D. Thomas⁸⁴, Andrew D. Thomas²⁸¹,
69 Katja Tielbörger⁶¹, Marcello Tomaselli⁶³, Urs Albert Treier^{34,35}, Mario Trouillier²¹⁷, Pavel Dan Turtureanu^{234,282,236},
70 Rosamond Tutton²⁸³, Vilna A. Tyystjärvi^{4,3}, Masahito Ueyama²⁸⁴, Karol Ujházy¹⁷⁹, Mariana Ujházyová⁷⁴, Domas
71 Uogintas²⁸⁵, Anastasiya Vladimirovna Urban^{218,185}, Josef Urban^{185,30}, Marek Urbaniak¹⁵³, Tudor-Mihai Ursu²⁸⁶,
72 Francesco Primo Vaccari²⁸⁷, Stijn Van de Vondel²⁸⁸, Liesbeth van den Brink⁶¹, Maarten Van Geel²⁸⁹, Vigdis
73 Vandvik¹³⁴, Pieter Vangansbeke⁷, Andrej Varlagin²⁹⁰, G.F. (Ciska) Veen²⁹¹, Elmar Veenendaal²⁹², Susanna E.
74 Venn²⁹³, Hans Verbeeck²⁹⁴, Erik Verbruggen¹, Frank G.A. Verheijen²⁹⁵, Luis Villar²⁹⁶, Luca Vitale²⁹⁷, Pascal
75 Vittoz²⁹⁸, Maria Vives-Inglá⁶⁵, Jonathan von Oppen^{34,35}, Josefine Walz⁹⁶, Runxi Wang¹²⁷, Yifeng Wang²⁸³, Robert
76 G. Way²⁸³, Ronja E. M. Wedegärtner¹²⁴, Robert Weigel¹⁴⁶, Jan Wild^{9,161}, Matthew Wilkinson⁴³, Martin
77 Wilmking²¹⁷, Lisa Wingate¹⁰⁴, Manuela Winkler¹⁶⁸, Sonja Wipf²⁴⁴, Georg Wohlfahrt¹³⁶, Georgios Xenakis²⁹⁹, Yan
78 Yang³⁰⁰, Zicheng Yu^{301,302}, Kailiang Yu³⁰³, Florian Zellweger¹¹², Jian Zhang^{304,305}, Zhaochen Zhang³⁰⁴, Peng Zhao¹⁵²,
79 Klaudia Ziemblińska¹⁵³, Reiner Zimmermann^{206,306}, Shengwei Zong³⁰⁷, Viacheslav I. Zyryanov²¹⁸, Ivan Nijs^{1,+},
80 Jonathan Lenoir^{272,+,x}

81 *Jonas J. Lembrechts and Johan Van den Hoogen should be considered joint first author

82 ⁺ Ivan Nijs and Jonathan Lenoir should be considered joint senior author

83 ^x Corresponding authors

84 ** See end of manuscript for affiliations

85

86 Corresponding authors

87 Jonas Lembrechts (Jonas.lembrechts@uantwerpen.be, <https://orcid.org/0000-0002-1933-0750>, +).

88 Jonathan Lenoir (jonathan.lenoir@u-picardie.fr, <https://orcid.org/0000-0003-0638-9582>).

89

90 **Abstract**

91 Research in global change ecology relies heavily on global climatic grids derived from
92 estimates of air temperature in open areas at around 2 m above the ground. These climatic
93 grids thus do not reflect conditions below vegetation canopies and near the ground surface,
94 where critical ecosystem functions are controlled and most terrestrial species reside. Here, we
95 we provide global maps of soil temperature and bioclimatic variables at a 1-km² resolution
96 for the 0–5 and 5–15 cm depth. These maps were created by calculating the difference (i.e.,
97 offset) between *in-situ* soil temperature measurements, based on time series from over 1200
98 1-km² pixels (summarized from 8500 unique temperature sensors) across all the world's
99 major terrestrial biomes, and coarse-grained air temperature estimates from ERA5-Land (an
100 atmospheric reanalysis by the European Centre for Medium-Range Weather Forecasts). We
101 show that mean annual soil temperature differs markedly from the corresponding 2 m
102 gridded air temperature, by up to 10°C (mean = $3.0 \pm 2.1^\circ\text{C}$), with substantial variation across
103 biomes and seasons. Over the year, soils in cold and/or dry biomes are substantially warmer
104 ($3.6 \pm 2.3^\circ\text{C}$ warmer than gridded air temperature), whereas soils in warm and humid
105 environments are on average slightly cooler ($0.7 \pm 2.3^\circ\text{C}$ cooler). The observed substantial and
106 biome-specific offsets underpin emphasize that the projected impacts of climate and climate
107 change on biodiversity and ecosystem functioning are inaccurately assessed when air rather
108 than soil temperature is used, especially in cold environments. The global soil-related
109 bioclimatic variables provided here are an important step forward for any application in
110 ecology and related disciplines. Nevertheless, we highlight the need to fill remaining global
111 gaps by collecting more *in-situ* measurements of microclimate conditions to further enhance
112 the spatiotemporal resolution of global soil temperature products for ecological applications.

113

114 **Keywords:** bioclimatic variables, global maps, microclimate, near-surface temperatures, soil-
115 dwelling organisms, soil temperature, temperature offset, weather stations

116 **Introduction**

117 With the rapidly increasing availability of big data on species distributions, functional traits
118 and ecosystem functioning (Bond-Lamberty & Thomson, 2018, Bruelheide *et al.*, 2018,
119 Kissling *et al.*, 2018, Kattge *et al.*, 2019, Lenoir *et al.*, 2020), we can now study biodiversity
120 and ecosystem responses to global changes in unprecedented detail (Senior *et al.*, 2019,
121 Steidinger *et al.*, 2019, Van Den Hoogen *et al.*, 2019, Antão *et al.*, 2020). However, despite
122 this increasing availability of ecological data, most spatially-explicit studies of ecological,
123 biophysical and biogeochemical processes still ~~make have to rely on~~ ~~use of~~ the same global
124 gridded temperature data (Soudzilovskaia *et al.*, 2015, Van Den Hoogen *et al.*, 2019, Du *et al.*,
125 2020). ~~Most of these gridded air temperature datasets are based on long-term climatologies~~
126 ~~of rather coarse spatiotemporal resolutions: monthly and annual means, or bioclimatic~~
127 ~~derivatives, based on 30-yr time series averaged within 1 km to 50 km grid cells. Additionally,~~
128 ~~these coarse temperature grids are~~ ~~All~~ ~~thus far, these global gridded products are~~
129 ~~constructed based upon~~ ~~on~~ measurements from standard meteorological stations that
130 record free-air temperature inside well-ventilated protective shields placed up to 2 m above-
131 ground in open, shade-free habitats, where abiotic conditions may differ substantially from
132 those actually experienced by most organisms (World Meteorological Organization, 2008,
133 Lembrechts *et al.*, 2020).

134 Ecological patterns and processes often relate more directly to below-canopy soil
135 temperature rather than to well-ventilated air temperature inside a weather station. Near-
136 surface, rather than air, temperature better predicts ecosystem functions like biogeochemical
137 cycling (e.g., organic matter decomposition, soil respiration and other aspects of the global
138 carbon balance) (Schimel *et al.*, 2004, Pleim & Gilliam, 2009, Portillo-Estrada *et al.*, 2016,
139 Hursh *et al.*, 2017, Gottschall *et al.*, 2019, Davis *et al.*, 2020, Perera-Castro *et al.*, 2020, Jian *et*
140 *al.*, 2021). Similarly, the use of soil temperature in correlative analyses or predictive models
141 may improve predictions of climate impacts on organismal physiology and behaviour, as well
142 as on population and community dynamics and species distributions (Körner & Paulsen, 2004,
143 Schimel *et al.*, 2004, Ashcroft *et al.*, 2008, Kearney *et al.*, 2009, Scherrer *et al.*, 2011, Opedal
144 *et al.*, 2015, Berner *et al.*, 2020, Zellweger *et al.*, 2020). Given the key role of soil-related
145 processes for both aboveground and belowground parts of the ecosystem and their
146 feedbacks to the atmosphere (Crowther *et al.*, 2016), adequate soil temperature data are

147 critical for a broad range of fields of study, such as ecology, biogeography, biogeochemistry,
148 agronomy, soil science and climate system dynamics. Nevertheless, existing global soil
149 temperature products such as those from ERA5-Land (Copernicus Climate Change Service
150 (C3S), 2019), with a resolution of 0.08×0.08 degrees ($\approx 9 \times 9$ km at the equator), remain too
151 coarse for most ecological applications.

152 The direction and magnitude of the – often multi-degree – difference or *offset* between *in-*
153 *situ* soil temperature and coarse-gridded air temperature products result from a combination
154 of two factors: (i) the (vertical) microclimatic difference between air and soil temperature,
155 and (ii) the (horizontal) mesoclimatic difference between air temperature in flat, cleared
156 areas (i.e., where meteorological stations are located) and air temperature within different
157 vegetation types (e.g., below a dense canopy of trees) or topographies (e.g., within a ravine
158 or on a ridge) (Lembrechts *et al.*, 2020, De Frenne *et al.*, 2021). In essence, the offset is thus
159 the combination of both the vertical and horizontal differences that result from factors
160 affecting the energy budget at the Earth's surface, principally radiative energy: the ground
161 absorbs radiative energy, which is transferred to the air by convective heat exchange,
162 evaporation and spatial variation in net radiation, and lower convective conductance near the
163 Earth's surface results in horizontal and vertical variation in temperature (Richardson, 1922,
164 Geiger, 1950). Both these vertical and horizontal differences in temperature vary significantly
165 across the globe and in time as a result of environmental conditions affecting the radiation
166 budget (e.g., as a result of topographic orientation, canopy cover or surface albedo),
167 convective heat exchange and evaporation (e.g., foliage density, variation in the degree of
168 wind shear caused by surface friction) and the capacity for the soil to store and conduct heat
169 (e.g., water content and soil structure and texture) (Geiger, 1950, Zhang *et al.*, 2008, Way &
170 Lewkowicz, 2018, De Frenne *et al.*, 2019).

171 While the physics of soil temperatures have long been well-understood (Richardson, 1922,
172 Geiger, 1950), the creation of high-resolution global gridded soil temperature products has
173 not been feasible before, *amongst others partially* due to the absence of detailed global *in-*
174 *situ* soil temperature measurements (Lembrechts & Lenoir, 2019, Lembrechts *et al.*, 2020).
175 Recently, however, the call for microclimate temperature data *with spatiotemporal*
176 *resolutions relevant to the studied organism and, most importantly, values* representative of
177 *in-situ* conditions (i.e., microhabitat) as experienced by *these* organisms *living close to the*

178 ground surface or in the soil has become more urgent (Bramer *et al.*, 2018), while global data
179 availability has rapidly increased (Lembrechts *et al.*, 2020). In this paper, we ~~mainly~~ address
180 ~~the point on the representativeness of *in situ* conditions~~ ~~this issue~~ by generating global
181 gridded maps of below-canopy and near-surface soil temperature at 1-km² resolution (in line
182 with most existing global air temperature products). These maps are more representative of
183 the habitat conditions as experienced by organisms living under vegetation canopies, in the
184 topsoil or near the soil surface. They were created using the abovementioned offset between
185 gridded air temperature data and *in-situ* soil temperature measurements. We expect these
186 soil temperature maps to be substantially more representative of actual microclimatic
187 conditions than existing products – even though still at a relatively coarse spatial resolution
188 of 1-km² and summarizing multi-decadal averages – as they capture relevant near-surface and
189 below-ground abiotic conditions where ecosystem functions and processes operate (Daly,
190 2006, Bramer *et al.*, 2018, Körner & Hiltbrunner, 2018). Indeed, the offset between free-air
191 (macroclimate) and soil (microclimate) temperature, and between cleared areas and other
192 habitats, can easily reach up to $\pm 10^{\circ}\text{C}$ annually, even at the coarse 1-km² spatial resolution
193 used here (Zhang *et al.*, 2018, Lembrechts *et al.*, 2019, Wild *et al.*, 2019).

194 To create the global gridded soil temperature maps introduced above, we used over 8500
195 time series of soil temperature measured *in-situ* across the world's major terrestrial biomes,
196 compiled and stored in the SoilTemp database (Lembrechts *et al.*, 2020) (Fig. 1a,
197 Supplementary Material Fig. S1) and averaged into 1200 (or 1000 for the second soil layer)
198 unique 1-km² pixels. First, to illustrate the magnitude of the studied effect, we visualized the
199 global and biome-specific patterns in the mean annual offset between *in-situ* soil temperature
200 (topsoil: 0–5 cm and second layer: 5–15 cm depth) and coarse-scale interpolated air
201 temperature from ERA5-Land (soil temperature minus air temperature, hereafter called the
202 *temperature offset*, sensu (De Frenne *et al.*, 2021); elsewhere called the *surface offset* (Smith
203 & Riseborough, 1996, Smith & Riseborough, 2002)) using the average within 1 × 1 km grid
204 cells. Next, we used a machine learning approach with 31 environmental explanatory
205 variables (including macroclimate, soil, topography, reflectance, vegetation and
206 anthropogenic variables) to model the spatial variation in monthly temperature offsets at a 1
207 × 1 km resolution for all continents except Antarctica (as absent in many of the used predictor
208 variable layers). Using these offsets, we then calculated relevant soil-related bioclimatic

209 variables (SBIO), mirroring the existing global bioclimatic variables for air temperature.
210 Finally, we compare our new global soil temperature product with a similar one calculated
211 using coarser-resolution soil temperature data from ERA5-Land (Copernicus Climate Change
212 Service (C3S), 2019).

213 **Methods**

214 ***Data acquisition***

215 Analyses are based on SoilTemp, a global database of microclimate time series (Lembrechts
216 *et al.*, 2020). We compiled soil temperature measurements from 9362 unique sensors (mean
217 duration 2.9 years, median duration 1.0 year, ranging from 1 month to 41 years) from 60
218 countries, using both published and unpublished data sources (Fig. 1, Supplementary Material
219 Fig. S1). Each sensor corresponds to one independent time series.

220 We used time series spanning a minimum of one month, with a temporal resolution of four
221 hours or less. Sensors of any type were included (Supplementary Material Table S1), as long
222 as they measured *in situ*. Sensors in experimentally manipulated plots, i.e., plots in which
223 microclimate has been manipulated, such as in open top chambers, were excluded. Most data
224 (> 90%) came from low-cost rugged microclimate loggers such as iButtons (Maxim Integrated,
225 USA) or TMS4-sensors (Wild *et al.*, 2019), with measurement errors of around 0.5–1°C (note
226 that we are using degree Celsius over Kelvin throughout, for ease of understanding), while
227 in a minority of cases sensors with higher meteorological specifications such as industrial or
228 scientific grade thermocouples and thermistors (measurement errors of less than 0.5°C) were
229 used. Contributing datasets mostly consisted of short-term regional networks of microclimate
230 measurements, yet also included a set (< 5%) of soil temperature sensors from long-term
231 research networks equipped with weather stations (e.g., Pastorello *et al.*, 2017). By combining
232 these two types of data, a much higher spatial density of sensors and broader distribution of
233 microhabitats could be obtained than by using weather station data only.

234 About 68% of sensors measured in time intervals located between 2010 and 2020 and 93%
235 between 2000 and 2020; we thus focus on the latter period in our analyses. Additionally, given
236 the relatively short time frame covered by most individual sensors and thus the lack of
237 spatially unbiased long-term time series, we were not able to test for systematic differences

238 in the temperature offset between old and recent data sets, and thus we did not correct for
239 this in our models. We strongly urge future studies to assess such temporal dynamics in the
240 offset, once long-term microclimate data have become sufficient and more available.

241 For each of the individual 9362 time series, we calculated monthly mean, minimum (5%
242 percentile of all monthly values) and maximum (95% percentile) temperature, after checking
243 all time series for plausibility and erroneous data. These monthly values, while perhaps not
244 fully intercomparable between the northern and southern hemisphere, are those that have
245 traditionally been used to calculate bioclimatic variables (Fick & Hijmans, 2017). Months with
246 more than one day of missing data, either at the beginning or end of the measurement period,
247 or due to logger malfunctioning during measurement, were excluded, resulting in a final
248 subset of 380–380,676 months of soil temperature time series that were used for further
249 analyses. For each sensor with more than twelve months of data, we calculated moving
250 averages of annual mean temperature, using each consecutive month as a starting month and
251 calculating the mean temperature including the next eleven months. We used these moving
252 averages to make maximal use of the full temporal extent covered by each sensor, because
253 each time series spanned a different time period, often including parts of calendar years only.
254 ~~Next, these moving averages were further summarized to one mean annual average per 1~~
255 ~~km² pixel (see below, under 'Global and biome-level analyses')~~.

256 The selected dataset contained sensors installed strictly belowground, measuring
257 temperature at depths between 0 and 200 cm below the ground surface. Sensors recording
258 several measurements at the same site but located at different (vertical) depths were
259 included separately (the 9362 unique sensors thus came from 7251 unique loggers).

260 Sensors were grouped in different soil depth categories (0–5, 5–15, 15–30, 30–60, 60–100,
261 100–200 cm, Supplementary Material Table S2) to incorporate the effects of soil temperature
262 dampening. We limited our analyses to the topsoil (0–5 cm) and the second soil layer (5–15
263 cm), as we currently lack sufficient global coverage to make trustworthy models at deeper
264 soil depths (8519 time series, about 91%, came from the two upper depth layers). Due to
265 uncertainty in identification of these soil depths between studies (e.g., due to litter layers),
266 no finer categorisation is used.

267 We tested for potential bias in temporal resolution (i.e., measurement interval) by calculating
268 mean, minimum and maximum temperature for a selection of 2000 months for data
269 measured every 15 minutes, and the same data aggregated to 30, 60, 90, 120 and 240
270 minutes. Monthly mean, minimum and maximum temperature calculated with any of the
271 aggregated datasets differed on average less than 0.2°C from the ones with the highest
272 temporal resolution. We were thus confident that pooling data with different temporal
273 resolutions of 4 hours or finer would not significantly affect our results.

274 ***Temperature offset calculation***

275 For each monthly value at each sensor location (see Supplementary Material Table S3 for
276 number of data points per month), we extracted the corresponding monthly means of the 2
277 m air temperature from the European Centre for Medium-Range Weather (ECMWF)
278 Forecast's 5th reanalysis (ERA5) (from 1979–1981) and ERA5-Land from 1981–2020
279 (Copernicus Climate Change Service (C3S), 2019), hereafter called ERA5L. The latter dataset
280 models the global climate with a spatial resolution of 0.08×0.08 degrees ($\approx 9 \times 9$ km at the
281 equator) with an hourly resolution, converted into monthly means using daily means for the
282 whole month. Similarly, monthly minima and maxima were obtained from TerraClimate
283 (Abatzoglou *et al.*, 2018) for the period 2000 to 2020 at a 0.04×0.04 degrees ($\approx 4 \times 4$ km at
284 the equator) resolution. Monthly means for TerraClimate were not available, and we
285 therefore estimated them by averaging the monthly minima and maxima. Finally, we also
286 obtained monthly mean temperatures from CHELSA (Karger *et al.*, 2017a, Karger *et al.*, 2017b)
287 for the period 2000 to 2013 at a 30×30 arc second ($\approx 1 \times 1$ km at the equator) resolution. In
288 our modelling exercises (see section '*Integrative modelling*' below), we opted to use the mean
289 temperature offsets as calculated based on ERA5L rather than on CHELSA. While CHELSA's
290 higher spatial resolution is definitely an advantage, its time period (stopping in 2013)
291 insufficiently overlapped with the time period covered by our *in-situ* measurements (2000 to
292 2020), soilso— temperature offsets based on the CHELSA dataset were only used for
293 comparative purposes. We used TerraClimate to model offsets in monthly minimum and
294 maximum temperature.

295 We calculated moving annual averages of the gridded air temperature data ~~similar in the~~
296 ~~same way as to those we computed~~ for soil temperature. These were used to create annual
297 temperature offset values following the same approach as above.

298 The offset between the *in situ* measured soil temperature in the SoilTemp database and the
299 2 m free-air temperature obtained from the air-temperature grids (ERA5L, TerraClim and
300 CHELSA, hereafter called 'gridded air temperature') was calculated by subtracting the
301 monthly or annual mean air temperature from the monthly or annual mean soil temperature.
302 Positive offset values indicate a measured soil temperature higher than gridded air
303 temperature, while negative offset values represent cooler soils. Similarly, monthly minimum
304 and maximum air temperature were subtracted from minimum and maximum soil
305 temperature, respectively. Monthly minima and maxima of the soil temperature were
306 calculated as, respectively, the 5% lowest and highest instantaneous measurement in that
307 month, to correct for outliers, which can be especially pronounced at the soil surface (Speak
308 *et al.*, 2020). As a result, patterns in minima and maxima are more conservative estimates
309 than if we had used the absolute lowest and highest values.

310 Importantly, the temperature offset calculated here is a result of three key groups of drivers:
311 (1) height effects (2 m versus 0–15 cm below the soil surface); (2) environmental or habitat
312 effects (e.g., spatial variability in vegetation, snow or topography); and (3) spatial scale effects
313 (resolution of gridded air temperature) (Lembrechts *et al.*, 2020). We investigated the
314 potential role of scale effects by comparing gridded air temperature data sources with
315 different resolutions (ERA5L, TerraClimate and CHELSA, see below). Height effects and
316 environmental effects are however not disentangled here, as the offset we propose
317 incorporates both the difference between air and soil temperature (vertically), as well as the
318 difference between free-air macroclimate and *in situ* microclimate (horizontally) in one
319 measure (Lembrechts *et al.*, 2020). While it can be argued that it would be better to treat
320 both vertical and horizontal effects separately, this would require a similar database of
321 coupled *in-situ* air and soil temperature measurements, which is not yet available. Using *in*
322 *situ* measured air temperature could also solve spatial mismatches (i.e., spatially averaged air
323 temperature represents the whole 1 to 81 km² pixel, depending on pixel size, not only the
324 exact location of the sensor). However, coupled air and soil temperature measurements are
325 not only rare, but the air temperature measurements also have large measurement errors,

326 especially in open habitats (Maclean *et al.*, 2021). These errors can be up to several degrees
327 in open habitats when using non-standardized sensors, loggers and shielding (Holden *et al.*,
328 2013, Terando *et al.*, 2017, Maclean *et al.*, 2021). Hence, using—*in situ* measured air
329 temperature without correcting for these measurement errors would be misleading.

330 ***Global and biome-level analyses***

331 For the purpose of visualization, annual offsets were first averaged in hexagons with a
332 resolution of approximately ~~70~~–70,000 km², using the dggridR-package ([version 2.0.4](#)) in R
333 (Barnes *et al.*, 2017) (Fig. 1). Next, we plotted mean, minimum and maximum annual soil
334 temperature as a function of corresponding gridded air temperature from ERA5, TerraClimate
335 and CHELSA and used generalized additive models (GAMs, package mgcv 1.8-31; Wood, 2012)
336 to visualise deviations from the 1:1-line (i.e., temperature offsets deviating from zero,
337 Supplementary Figs. S4-5).

338 All annual and monthly values within each soil depth category and falling within the same 1-
339 km² pixel were aggregated as a mean, resulting in a total of c. 1200 unique pixels at 0–5 cm,
340 and c. 1000 unique pixels at 5–15 cm each month, across the globe (Supplementary Material
341 Table S3). This averaging includes summarizing the data over space, i.e., multiple sensors
342 within the same 1-km² pixel, and time, i.e., data from multi-year time series from a certain
343 sensor, to reduce spatial and temporal autocorrelation and sampling bias. We assigned these
344 1-km² averages to the corresponding Whittaker biome of their georeferenced location, using
345 the package *plotbiomes* ([version 0.0.0.9901](#)) in R (Fig. 1 c, d, Supplementary Material Table
346 S4-5 (Stefan & Levin, 2018)). We ranked biomes based on their offset and compared this with
347 the mean annual precipitation in each biome (Fig. 1b). This was done separately for each air
348 temperature data source (ERA5L, TerraClimate and CHELSA), soil depth (0–5 cm, 5–15 cm)
349 and timeframe (ERA5L 1979–2020, 2000–2020), as well as for the offset between monthly
350 minimum and maximum soil temperature and the minimum and maximum gridded air
351 temperature from TerraClimate. Our analyses showed that patterns were robust to variation
352 in spatial resolution, sensor depth, climate interpolation method and temporal scale
353 (Supplementary Material Figs. S2–5).

354 ***Acquisition of global predictor variables***

355 To create spatial predictive models of the offset between *in-situ* soil temperature and gridded
356 air temperature, we first sampled a stack of global map layers at each of the logger locations
357 within the dataset. These layers included long-term macroclimatic conditions, soil texture and
358 physiochemical information, vegetation, radiation, and topographic indices as well as
359 anthropogenic variables. Details of all layers, including descriptions, units, and source
360 information, are described in Supplementary Data S1. In short, information about soil texture,
361 structure and physiochemical properties was obtained from SoilGrids (version 1 (Hengl *et al.*,
362 2017)), limited to the upper soil layer (top 5 cm). Long-term averages of macroclimatic
363 conditions (i.e., monthly mean, maximum and minimum temperature, monthly precipitation)
364 was obtained from CHELSA (version 2017 (Karger *et al.*, 2017a)), which includes climate data
365 averaged across 1979–2013, and from WorldClim (version 2 (Fick & Hijmans, 2017)). Monthly
366 snow probability is based on a pixel-wise frequency of snow occurrence (snow cover >10%)
367 in MODIS daily snow cover products (MOD10A1 & MYD10A1 (Hall *et al.*, 2002)) in 2001–2019.
368 Spectral vegetation indices (i.e., averaged MODIS NDVI product MYD13Q1) and surface
369 reflectance data (i.e., MODIS MCD43A4) were obtained from the Google Earth Engine Data
370 Catalog (developers.google.com/earth-engine/datasets) and averaged from 2015 to 2019.
371 Landcover and topographic information were obtained from EarthEnv (Amatulli *et al.*, 2018).
372 Aridity index (AI) and potential evapotranspiration (PET) layers were obtained from CGIAR
373 (Zomer *et al.*, 2008). Anthropogenic information (population density) was obtained from the
374 EU JRC (ghsl.jrc.ec.europa.eu/ghs_pop2019.php). Aboveground biomass data were obtained
375 from GlobBiomass (Santoro, 2018). ~~Resolved~~ RESOLVE ecoregion classifications were used to
376 categorize sampling locations into biomes (Dinerstein *et al.*, 2017). With this set of predictor
377 variables, we included information on all different categories of drivers of soil temperature.
378 An important variable that had to be excluded was snow depth, due to the lack of a relevant
379 1-km² resolution global product. The final set of predictor variables included 24 'static'
380 variables and eight monthly layers (i.e., maximum, mean, and minimum temperature,
381 precipitation, cloud cover, solar radiation, water vapour pressure, and snow cover). As cloud
382 cover estimates were not available for high-latitude regions in the Northern Hemisphere in
383 January and December due to a lack of daylight, we excluded cloud cover as an explanatory
384 variable for these months (i.e., 'EarthEnvCloudCover_MODCF_monthlymean_XX', with XX
385 representing the months in two-digit form Supplementary Data S1).

386 All variable map layers were reprojected and resampled to a unified pixel grid in EPSG:4326
387 (WGS84) at 30 arc-sec resolution ($\approx 1 \times 1$ km at the equator). Areas covered by permanent
388 snow or ice (e.g., the Greenland ice cap or glaciated mountain ranges, identified using
389 SoilGrids) were excluded from the analyses. Antarctic sampling points were excluded from
390 the modelling data set owing to the limited coverage of several covariate layers in the region.

391 ***Integrative modelling***

392 To generate global maps of monthly temperature offsets (Fig. 2), we trained ~~R~~andom ~~F~~orest
393 (RF) models for each month, using the temperature offsets as the response variables and the
394 global variable layers as predictors (Hengl *et al.*, 2018). We used a geospatial RF modelling
395 pipeline as developed by van den Hoogen *et al.* (2021). RF models are a type of machine
396 learning model that combines many classification trees using randomized subsets of the data,
397 with each tree iteratively dividing data into groups of most closely related data points (Hengl
398 *et al.*, 2018). They are particularly valuable here due to their capacity to uncover nonlinear
399 relationships (e.g., due to increased decoupling of soil from air temperature in colder and thus
400 snow-covered areas) and their ability to capture complex interactions among covariates (e.g.,
401 between snow and vegetation cover) (Olden *et al.*, 2008). Furthermore, they may currently
402 have advantages over mechanistic microclimate models for global modelling (Maclean &
403 Klinges, 2021), as the latter require highly detailed physical input parameters for calibration,
404 and currently too much computational time to cover the globe at a 1 km² resolution and over
405 multiple decades. Nevertheless, we urge future endeavours to compare and potentially
406 improve our results with estimates based on such mechanistic models.

407 We performed a grid search procedure to tune the RF models across a range of ~~122–52~~
408 hyperparameter settings (variables per split: 2–~~142~~, minimum leaf population: 2–~~512~~, in all
409 combinations adding up to 12152 models, each time with 250 trees). During this procedure,
410 we assessed each of the 52 model's performance using k-fold cross-validation ($k = 10$; folds
411 assigned randomly, stratified per biome), ~~for each of the 122 models~~. The models' mean and
412 standard deviation values were the basis for choosing the best of all evaluated models. This
413 procedure was repeated for each month separately for the two soil depth layers (0–5 cm, 5–
414 15 cm), for offsets in mean, minimum and maximum temperature. The importance of
415 explanatory variables was assessed using the variable importance and ordered by mean

416 variable importance across all models. This variable importance adds up the decreases in the
417 impurity criterion (i.e., the measure on which the local optimal condition is chosen) at each
418 split of a node for each individual variable over all trees in the forest (van den Hoogen *et al.*,
419 2021).

420 ***Soil bioclimatic variables***

421 The resulting global maps of the annual and monthly offsets between mean, minimum and
422 maximum soil and air temperature were used to calculate relevant bioclimatic variables
423 following the definition used in CHELSA, BIOCLIM, ANUCLIM and WorldClim (Xu & Hutchinson,
424 2011, Booth *et al.*, 2014, Fick & Hijmans, 2017, Karger *et al.*, 2017a) (Fig. 3–4). We calculated
425 11 soil bioclimatic layers (SBIO, Table 1). First, we calculated monthly soil mean, maximum
426 and minimum temperature by adding monthly temperature offsets to the respective CHELSA
427 monthly mean, maximum and minimum temperature (Karger *et al.*, 2017a). Next, we used
428 these soil temperature layers to compute the SBIO layers (O'Donnell & Ignizio, 2012). Wettest
429 and driest quarters were identified for each pixel based on CHELSA's monthly values.

430 ***Model uncertainty***

431 To assess the uncertainty in the monthly models, we performed a stratified bootstrapping
432 procedure, with total size of the bootstrap samples equal to the original training data (van
433 den Hoogen *et al.*, 2021). Using biomes as a stratification category, we ensured the samples
434 included in each of the bootstrap training collections were proportionally representative of
435 each biome's total area. Next, we trained RF models (with the same hyperparameters as
436 selected during the grid-search procedure) using each of 100 bootstrap iterations. Each of
437 these trained RF models was then used to classify the covariate layer stack, to generate per-
438 pixel 95% confidence intervals and standard deviation for the modelled monthly offsets (Fig.
439 5a, Supplementary Material Fig. S6a). The mean R^2 value of the RF models for the monthly
440 mean temperature offset was 0.70 (from 0.64 to 0.78) at 0–5 cm and 0.76 (0.63–0.85) at 5 to
441 15 cm across all twelve monthly models. Mean RMSE of the models was 2.20°C (1.94–2.51°C)
442 at 0–5 cm, and 2.06°C (1.67–2.35°C) at 5–15 cm.

443 Importantly, model uncertainty as reported in Fig. 5a and Supplementary Material Fig. S6a
444 comes on top of existing uncertainties in (1) *in-situ* soil temperature measurements and (2)

445 the ERA5L macroclimate models as used in our models. However, both of those are usually
446 under 1°C (Copernicus Climate Change Service (C3S), 2019, Wild *et al.*, 2019).

447 To assess the spatial extent of extrapolation, which is necessary due to the incomplete global
448 coverage of the training data, we first performed a Principal Component Analysis (PCA) on the
449 full environmental space covered by the monthly training data, including all explanatory
450 variables as used in the models, and then transformed the composite image into the same PC
451 spaces as of the sampled data (Van Den Hoogen *et al.*, 2019). Next, we created convex hulls
452 for each of the bivariate combinations from the first 10 to 12 PCs, covering at least 90% of the
453 sample space variation, with the number of PCs depending on the month. Using the
454 coordinates of these convex hulls, we assessed whether each pixel fell within or outside each
455 of these convex hulls, and calculated the percentage of bivariate combinations for which this
456 was the case (Fig. 5b, Supplementary Material Fig. S6b). This process was repeated for each
457 month, and for each of the two soil depths separately.

458 These uncertainty maps are important because one should be careful with extrapolation
459 beyond the range of conditions covered by the environmental variables included in the
460 original calibration dataset, especially in the case of non-linear patterns such as modelled
461 here. The maps are provided as spatial masks to remove or reduce the weighting of the pixels
462 for which predictions are beyond the range of values covered by the models during
463 calibration. To assess this further, we used a spatial leave-one-out cross-validation analysis to
464 test for spatial autocorrelation in the data set (Supplementary Material Fig. S7) (van den
465 Hoogen *et al.*, 2021). This approach trains a model for each sample in the data set on all
466 remaining samples, excluding data points that fall within an increasingly large buffer around
467 that focal sample. Results show lowest confidence for May to September at 5–15 cm, likely
468 driven by uneven global coverage of data points.

469 Finally, we compared the modelled mean annual temperature (SBIO1, topsoil layer) with a
470 similar product based on monthly ERA5L topsoil (0–7 cm) temperature with a spatial
471 resolution of 0.1 × 0.1 degrees (Copernicus Climate Change Service (C3S), 2019). The
472 corresponding SBIO1 based on ERA5L was calculated using the means of the monthly
473 averages for each month over the period 1981 to 2016, and averaging these 12 monthly
474 values into one annual product. We then visualized spatial differences between SBIO1 and

475 ERA5, as well as differences across the macroclimatic gradient, to identify mismatches
476 between both datasets.

477 All geospatial modelling was performed using the Python API in Google Earth Engine (Gorelick
478 *et al.*, 2017). The R statistical software, version 4.0.2 (R Core Team, 2020), was used for data
479 visualisations. All maps were plotted using the Mollweide projection (which preserves relative
480 areas) to avoid large distortions at high latitudes.

481 ***Sources of uncertainty***

482 There is a temporal mismatch between the period covered by CHELSA (1979-2013) and our
483 *in-situ* measurements (2000-2020), which prevented us from directly using CHELSA climate to
484 calculate the temperature offsets used in our models. This temporal mismatch might affect
485 the offsets calculated here because the relationship between temperature offset and
486 macroclimate will change through time as the climate warms. Similarly, inter-annual
487 differences in offsets due to specific weather conditions cannot be implemented in the used
488 approach. However, we are confident that at the relatively coarse spatial (1 km²) and
489 temporal (monthly averages) resolution we are working at, our results are sufficiently robust
490 to withstand ~~this-these temporal issuesmismatch~~, given that we found high consistency in
491 offset patterns between the different timeframes and air temperature datasets examined
492 (Supplementary Material Figs. S2–5). Nevertheless, we strongly urge future research to
493 disentangle these potential temporal dynamics, especially given the increasing rate at which
494 the climate is warming (Xu *et al.*, 2018, GISTEMP Team, 2021).

495 Similarly, a potential bias could result from the mismatch in method and resolution between
496 ERA5L – used to calculate the temperature offsets – and CHELSA, which was used to create
497 the bioclimatic variables. However, even though temperature offsets have slightly larger
498 variation when based on the coarser-grained ERA5L-data than on the finer-grained CHELSA-
499 data, Supplementary Material Figs. S2–5 show that relationships between soil and air
500 temperature are largely consistent in all biomes and across the whole global temperature
501 gradient. Therefore, the larger offsets created additional random scatter, yet no consistent
502 bias.

503 Finally, we acknowledge that the 1-km² resolution gridded products might not be
504 representative of conditions at the *in-situ* measurement locations within each pixel. This issue
505 could be particularly significant for different vegetation types (here proxied at the pixel level
506 using total aboveground biomass (unit: tons/ha i.e., Mg/ha, for the year 2010; Santoro, 2018)
507 and NDVI (MODIS NDVI product MYD13Q1, averaged over 2015–2019)). To verify this, we
508 compared a pixel's estimated aboveground biomass with the dominant *in-situ* habitat (forest
509 versus open) surrounding the sensors in that- pixel (Supplementary Table S6). Importantly, all
510 sensors installed in forests fell indeed in pixels with more than 1 ton/ha aboveground
511 biomass. Similarly, 75% or more of sensors in open terrain fell in pixels with biomass estimates
512 of less than 1 ton/ha. Only in the temperate woodland biome was the match between *in-situ*
513 habitat estimates and pixel-level aboveground biomass lower, with less than 95% of sensors
514 in forested locations correctly placed in pixels with more than 1 ton/ha biomass, and less than
515 50% of open terrain sensors in pixels with less than 1 ton/ha biomass. While our predictions
516 will thus not be accurate for locations within a pixel that largely deviate from average
517 conditions (e.g., open terrain in pixels identified as largely forested, or vice versa), they should
518 be largely representative for those pixel-level averages.

519 **Results**

520 ***Biome-wide patterns in the temperature offset***

521 We found positive and negative temperature offsets of up to 10°C between *in situ* measured
522 mean annual topsoil temperature and gridded air temperature (mean = $3.0 \pm 2.1^\circ\text{C}$ standard
523 deviation, Fig. 1, 0–5 cm depth; 5–15 cm is available in Supplementary Material Figs. S2, 5).
524 The magnitude and direction of these temperature offsets varied considerably within and
525 across biomes. Mean annual topsoil temperature was on average $3.6 \pm 2.3^\circ\text{C}$ higher than
526 gridded air temperature in cold and/or dry biomes, namely tundra, boreal forests, temperate
527 grasslands, and subtropical deserts. In contrast, offsets were slightly negative in warm and
528 wet biomes (tropical savannas, temperate forests, and tropical rainforests) where soils were,
529 on average, $0.7 \pm 2.7^\circ\text{C}$ cooler than gridded air temperature (Fig. 1b, Supplementary Material
530 Figs. S2 and 5; note, however, the lower spatial coverage in these biomes in Fig. 1a, c, d,
531 Supplementary Material Table S4). Temperature offsets in annual minimum and maximum
532 temperature amounted to c. 10°C maximum. While annual soil temperature minima were on

533 average higher than corresponding gridded air temperature minima in all biomes,
534 temperature offsets of annual maxima followed largely the same biome-related trends as
535 seen for the annual means, albeit with the higher variability expected for temperature
536 extremes (Supplementary Material Figs. S2g, h, S4g, h). Using different air temperature data
537 sources did not alter the annual temperature offset and biome-related patterns (see Methods
538 and Supplementary Material Figs. S2–5).

539 Soils in the temperate seasonal forest biome were on average 0.8°C (± 2.2°C) cooler than air
540 temperature within 1-km² grid cells of forested habitats, and 1.0°C (± 4.0°C) warmer than the
541 air within 1-km² grid cells of non-forested habitats, resulting in a biome-wide average of 0.5°C
542 (Supplementary Material Table S7). Similar patterns were observed in other biomes.

543 ***Temporal and spatial variation in temperature offsets***

544 Our ~~R~~andom ~~F~~orest modelling approach highlighted a strong seasonality in monthly
545 temperature offsets, especially towards higher latitudes (Fig. 2). High-latitude soils were
546 found to be several degrees warmer than the air (monthly offsets of up to 25°C) during their
547 respective winter months, and cooler (up to 10°C) in summer months, both at 0–5 cm (Fig. 2)
548 and 5–15 cm (Supplementary Material Fig. S8) soil depths. In the tropics and subtropics, soils
549 in dry biomes (e.g., in the Sahara Desert or southern Africa) were predicted to be warmer
550 than air throughout most of the year, whilst soils in mesic biomes (e.g., tropical biomes in
551 South America, central Africa and Southeast Asia) were modelled to be consistently cooler, at
552 both soil depths. These global gridded products were then used to create temperature-based
553 global bioclimatic variables for soils (SBIO, Fig. 3, Supplementary Material Fig. S9).

554 ***Global variation in soil temperature***

555 We observed 17% less spatial variation in mean annual soil temperature globally (expressed
556 by the standard deviation) than in air temperature, largely driven by the positive offset
557 between soil and air temperature in cold environments (Fig. 4). Importantly, our machine
558 learning models slightly (up to 1°C, or around 10% of variation) underestimated temperature
559 offsets at both extremes of the temperature gradient at the 1-km² resolution (Supplementary
560 Material Fig. S10) and likely even more in comparison with finer-resolution products.
561 Estimates of the reduction in variation across space are thus conservative, especially in the
562 coldest biomes. The reduction in spatial temperature variation was observed in all cold and

563 cool biomes, with tundra and boreal forests having both a significant positive mean
564 temperature offset and a reduction of 20% and 22% in variation, respectively (Fig. 4c). In the
565 warmest biomes (e.g., tropical savanna and subtropical desert), however, we found an
566 increase in variation of, on average, 10%.

567 Our bootstrap approach to validate modelled monthly offsets indicated high consistency
568 among the outcomes of 100 bootstrapped models (Fig. 5, Supplementary Material Fig. S6a),
569 with standard deviations in most months and across most parts of the globe around or below
570 $\pm 1^{\circ}\text{C}$. One exception to this was the temperature offset at high latitudes of the northern
571 hemisphere during winter months (standard deviation up to $\pm 5^{\circ}\text{C}$ in the 0–5 cm layer).
572 Predictive performance was comparable across biomes, although with large variation in data
573 availability (Supplementary Material Fig. S11).

574 The importance of explanatory variables in the RF models was largely consistent across
575 months. Macroclimatic variables such as incoming solar radiation as well as long-term
576 averages in air temperature and precipitation were by far the most influential explanatory
577 variables in the spatial models of the monthly temperature offset (Supplementary Material
578 Figs. S12, 13).

579 We highlight that the current availability of *in-situ* soil temperature measurements is
580 significantly lower in the tropics (Supplementary Material Table S5), where our model had to
581 extrapolate temperatures beyond the range used to calibrate the model (Fig. 5b,
582 Supplementary Material Fig. S6b).

583 Finally, our comparison with a mean annual soil temperature product derived from the
584 coarse-resolution ERA5L topsoil temperature showed that spatial variability, e.g., driven by
585 topographic heterogeneity, is much better captured here than in the coarser resolution of the
586 ERA5L-based product (Fig. 6c-e). Nevertheless, our predictions at the coarse scale showed to
587 be condensed within a 5°C range of values from the ERA5L-predictions, for more than 95% of
588 pixels globally. Noteworthy, our predictions resulted in consistently cooler soil temperature
589 predictions than topsoil conditions provided by ERA5L across large areas, such as the boreal
590 and tropical forest biomes (Fig. 6a, b). Additionally, our models predicted lower values for
591 SBIO1 than ERA5L in all regions with mean annual soil temperature below 0°C, except for a
592 few locations around Greenland and Svalbard (Fig. 6a, b).

593 **Discussion**

594 ***Global patterns in soil temperature***

595 We observed large spatiotemporal heterogeneity in the global offset between soil and air
596 temperature, often in the order of several degrees annually and up to more than 20°C during
597 winter months at high latitudes. These values are in line with empirical data from regional
598 studies (Zhang *et al.*, 2018, Lembrechts *et al.*, 2019, Obu *et al.*, 2019). Both annual and
599 monthly offsets showed clear discrepancies between cold and dry versus warm and wet
600 biomes. The modelled monthly offsets covaried strongly negatively with both long-term
601 averages in free-air temperature and solar radiation, linking to the well-known decoupling of
602 soil from air temperature due to snow (for cold extremes in cold and cool biomes) (Grundstein
603 *et al.*, 2005). However, the secondary importance of variables related to precipitation and soil
604 structure hints to the additional distinction between wet and dry biomes at the warm end of
605 the temperature gradient. There, where, buffering due to shading, evapotranspiration and
606 the specific heat of water (mostly against warm extremes in warm and wet biomes) results in
607 cooler soil temperature (Geiger, 1950, Grundstein *et al.*, 2005, Hennon *et al.*, 2010, Wang &
608 Dickinson, 2012, De Frenne *et al.*, 2013, Grünberg *et al.*, 2020), while such buffering is not as
609 strong in warm and dry biomes due to the lower water availability (Wang & Dickinson, 2012,
610 Greiser *et al.*, 2018, Zhou *et al.*, 2021). As such, these results highlight strong macroclimatic
611 impacts on the soil microclimate across the globe (see also De Frenne *et al.*, 2019), yet with
612 soil temperature importantly non-linearly related to air temperature at the global scale. This
613 confirms that the latter is not sufficient as a proxy for temperature conditions near or in the
614 soil. With our soil-specific global bioclimatic products, we have provided the means to correct
615 for these important region-specific, non-linear differences between soil and air temperature
616 at an unprecedented spatial resolution.

617 ***Drivers of the temperature offset***

618 Our empirical modelling approach enabled us to accurately map global patterns in soil
619 temperature. In doing so we did not aim to disentangle the mechanisms governing the
620 temperature offset: such an endeavour would require modelling the biophysics of energy
621 exchange at the soil surface across biomes (Kearney *et al.*, 2019, Maclean *et al.*, 2019,
622 Maclean & Klings, 2021). Importantly, many of the predictor variables used in our study (e.g.,

623 long-term averages in macroclimatic conditions or solar radiation) are unlikely to represent
624 direct causal relationships underlying the temperature offset, but may rather indirectly relate
625 to many ensuing factors that affect the functioning of ecosystems at fine spatial scales which,
626 in turn, feedback on local temperature offsets, such as energy and water balances, snow
627 cover, wind intensity and vegetation cover (De Frenne *et al.*, 2021). For example, while
628 increased solar radiation itself would theoretically result in soils warming more than the air,
629 high solar radiation at the global scale often coincides with high vegetation cover blocking
630 radiation input to the soil, thus correlating with relatively cooler soils (De Frenne *et al.*, 2021).
631 Our results highlight, however, that the complex relationship between microclimatic soil
632 temperature and macroclimatic air temperature is predictable across large spatial extents
633 thanks to broad scale patterns, even if this is governed by a multitude of local-scale factors
634 involving fine spatiotemporal resolutions. Nevertheless, the predictive quality of our models
635 was lower in high latitude regions, where high variation in the *in situ* measured offsets – likely
636 driven by the interactions between snow, local topography and vegetation – reduced
637 predictive power of the models at the 1-km² resolution (Greiser *et al.*, 2018, Way &
638 Lewkowicz, 2018, Grünberg *et al.*, 2020, Myers-Smith *et al.*, 2020, Niittynen *et al.*, 2020).

639 **Implications for microclimate warming**

640 Our results highlight clear biome-specific differences in mean annual temperature between
641 air and soil temperatures, as well as a significant reduction in the spatial variation in
642 temperature in the soil or near the soil surface, especially in cold and cool biomes (Fig. 4).
643 These patterns remain even despite the presence of often strongly opposing monthly offset
644 trends (Fig. 2). The observed correlation between long-term averages in macroclimatic
645 conditions and the annual temperature offset illustrates that soil temperature is unlikely to
646 warm at the same rate as air temperature when macroclimate warms. Indeed, one degree of
647 air temperature warming could result in either a bigger or smaller soil temperature change,
648 depending on where along the macroclimatic gradient this is happening. These effects might
649 be seen in cold biome soils most strongly, as they not only experience the largest (positive)
650 temperature offsets and reductions in climate range compared to air temperature (Fig. 4b, c),
651 but they are also expected to experience the strongest magnitude of macroclimate warming
652 (Cooper, 2014, Overland *et al.*, 2014, Chen *et al.*, 2021, GISTEMP Team, 2021). As a result,

653 mean annual temperatures in cold climate soils can be expected to warm slower than the
654 corresponding macroclimate as offsets shrink with increasing macroclimate warming.

655 Contrastingly, predicted climate warming in hot and dry biomes could be amplified in the
656 topsoil, where we show soils to become increasingly warmer than the air at higher
657 temperatures. Similarly, changes in precipitation regimes – and thus soil moisture – can
658 significantly alter the relationship between air and soil temperature, with critical implications
659 for soil moisture-atmosphere feedbacks, especially in hot biomes (Zhou *et al.*, 2021). Indeed,
660 as precipitation decreases, offsets could turn more positive and soil temperatures might
661 warm even faster than the observed macroclimate warming. Therefore, future research
662 should not only use soil temperature data as provided here to study belowground ecological
663 processes (De Frenne *et al.*, 2013, Lembrechts *et al.*, 2020), it should also urgently investigate
664 future scenarios of soil climate warming in light of changing air temperature and precipitation,
665 at ecologically relevant spatial and temporal resolutions to incorporate the non-linear
666 relationships exposed so far (Lembrechts & Nijs, 2020).

667 **Within-pixel heterogeneity**

668 We chose to use a 1-km² resolution spatial grid to model mismatches between soil and air
669 temperature, aggregating all values from different microhabitats within the same 1-km² grid
670 cell (e.g., sensors in forested versus open patches) as well as all daily and diurnal variation
671 within a month. Additionally, we used coarse-grained free-air temperature rather than in-situ
672 measured air temperatures. –We are aware that higher spatiotemporal resolutions would
673 likely reveal the importance of locally heterogeneous variables. Finer-scale factors that affect
674 the local radiation balance and wind (e.g., topography, snow and vegetation cover,
675 urbanization) at the landscape to local scales and those that directly affect neighbouring
676 locations (e.g. topographic shading and cold-air drainage, Whiteman, 1982, Ashcroft & Gollan,
677 2012, Lembrechts *et al.*, 2020) would probably have emerged as more important drivers at
678 regional scales and with higher spatiotemporal resolutions than those used here
679 (Supplementary Material Fig. S12). The latter is illustrated by the multi-degree Celsius
680 difference in mean annual temperature between forested and non-forested locations within
681 the same biome (Supplementary Material Table S7), as well as the lower accuracy obtained
682 during winter months at high latitudes, where and when fine-scale spatial heterogeneity in
683 snow cover and depth probably lowers models' predictability at the 1-km² resolution. *In-situ*

684 measurements were largely from areas with a representative vegetation type, supporting the
685 reliability of our predictions for the dominant habitat type within a pixel. However, improved
686 accuracy at high latitudes will depend on the future development of high-resolution snow
687 depth and/or snow water equivalent estimates (Luoju *et al.*, 2010).

688 The SoilTemp database (Lembrechts *et al.*, 2020) will facilitate the necessary steps towards
689 mapping soil temperature at higher spatiotemporal resolutions in the future, with its
690 georeferenced time series of *in situ* measured soil and near-surface temperature and
691 associated metadata. Nevertheless, when compared to existing soil temperature products
692 such as those from ERA5L (Copernicus Climate Change Service (C3S), 2019), we emphasize
693 that the increased resolution of our data products already provides a major technical
694 advance, even though substantial finer within-pixel variation is still lost through
695 spatiotemporal aggregation.

696 **Conclusions**

697 The spatial (biome-specific) and temporal (seasonally variable) offsets between air and soil
698 temperature quantified here likely bias predictions of current and future climate impacts on
699 species and ecosystems (Körner & Paulsen, 2004, Kearney *et al.*, 2009, Cooper, 2014, Opedal
700 *et al.*, 2015, Graae *et al.*, 2018, Zellweger *et al.*, 2020, Bergstrom *et al.*, 2021). Temperature
701 in the topsoil rather than in the air ultimately defines the distribution and performance of
702 most terrestrial species, as well as many ecosystem functions at or below the soil surface
703 (Pleim & Gilliam, 2009, Portillo-Estrada *et al.*, 2016, Hursh *et al.*, 2017, Gottschall *et al.*, 2019).
704 As many ecosystem functions are highly correlated with temperature (yet often non-linearity,
705 Johnston *et al.*, 2021), soil temperature rather than air temperature should in those instances
706 be the preferred predictor for estimating their rates and temperature thresholds (Rosenberg
707 *et al.*, 1990, Coûteaux *et al.*, 1995, Schimel *et al.*, 1996). Correcting for the non-linear
708 relationship between air and soil temperature identified here is thus vital for all fields
709 investigating abiotic and biotic processes relating to terrestrial environments (White *et al.*,
710 2020). Indeed, soil temperature, macroclimate and land-use change will interact to define the
711 future climate as experienced by organisms, and high-resolution soil temperature data is
712 needed to tackle current and future challenges.

713 By making our global soil temperature maps and the underlying monthly offset data openly
714 available, we offer gridded soil temperature data for climate research, ecology, agronomy
715 and other life and environmental sciences. Future research has the important task of further
716 improving the spatial and temporal resolution of global microclimate products as
717 microclimate operates at much higher temporal resolutions, with temporal variation over
718 hours, days, seasons and years (Potter *et al.*, 2013, Bütkofer *et al.*, 2020), as well as to confirm
719 accuracy of predictions in undersampled regions in the underlying maps (Lembrechts *et al.*,
720 2021). However, we are convinced that the maps presented here bring us one step closer to
721 having accessible climate data exactly where it matters most for many terrestrial organisms
722 (Kearney & Porter, 2009, Ashcroft *et al.*, 2014, Pincebourde *et al.*, 2016, Niittynen & Luoto,
723 2018, Lembrechts & Lenoir, 2019). We nevertheless highlight that there is still a long way to
724 go towards global soil microclimate data with an optimal spatiotemporal resolution. We
725 therefore urge all scientists to submit their microclimate time series to the SoilTemp database
726 to fill data gaps and help to increase the spatial resolution until it matches with the scale at
727 which ecological processes take place (Bütkofer *et al.*, 2020, Lembrechts *et al.*, 2020).

728

729 **Data availability**

730 All monthly data to train the models and reproduce the figures, sampled covariate data, and
731 models are available at <https://doi.org/10.5281/zenodo.4558663>. Soil bioclim layers SBIO1-
732 11 are also directly available in Google Earth Engine under
733 projects/crowtherlab/soil_bioclim/soil_bioclim_0_5cm and
734 projects/crowtherlab/soil_bioclim/soil_bioclim_5_15cm.

735

736 **Code availability**

737 All source code is available at <https://doi.org/10.5281/zenodo.4558663>.

738

739 **Acknowledgements**

740 JJL received funding from the Research Foundation Flanders (grant nr. 12P1819N) The project received funding from the Research
741 Foundation Flanders (grants nrs, G018919N, W001919N). JA received funding from the University of Helsinki, Faculty of Science
742 (MICROCLIM, grant nr. 7510145) and Academy of Finland Flagship (grant no. 337552). PDF, CM and PV received funding from the
743 European Research Council (ERC) under the European Union's Horizon 2020 research and innovation programme (ERC Starting Grant

744 FORMICA 757833). JK received funding from the Arctic Interactions at the University of Oulu and Academy of Finland (318930, Profi 4),
745 Maa- ja vesitekniikan tuki ry., Tiina and Antti Herlin Foundation, Nordenskiöld Samfundet and Societas pro Fauna et Flora Fennica. MK
746 received funding from the Czech Science Foundation (grant nr. 20-28119S) and the Czech Academy of Sciences (grant nr. RVO 67985939).
747 TC received funding from DOB Ecology. National Geographic Society grant no. 9480-14 and WW-240R-17. MA received funding from CISSC
748 (program ICRP (grant nr:2397) and INSF (grant nr: 96005914). The Royal Botanic Garden Edinburgh is supported by the Scottish
749 Government's Rural and Environment Science and Analytical Services Division. JMA received funding from the Funding Org. Qatar
750 Petroleum (grant nr. QUEX-CAS-QP-RD-18/19). JMA received funding from the European Union's Horizon 2020 research and innovation
751 program (grant no. 678841) and from the Swiss National Science Foundation (grant no. 31003A_176044). JA was supported by research
752 grants LTAUSA19137 (program INTER-EXCELLENCE, subprogram INTER-ACTION) provided by Czech Ministry of Education, Youth and Sports
753 and 20-05840Y of the Czech Science Foundation. AA was supported by the Ministry of Science and Higher Education of the Russian
754 Federation (grant FSRZ-2020-0014). SN, UAT, JJA, and JvO received funding from the Independent Research Fund Denmark (7027-00133B).
755 LvDB, KT, MYB and RC acknowledge funding from the German Research Foundation within the Priority Program SPP-1803 "EarthShape:
756 Earth Surface Shaping by Biota" (grant TI 338/14-1&2 and BA 3843/6-1). PB was supported by grant project VEGA of the Ministry of
757 Education of the Slovak Republic and the Slovak Academy of Sciences No. 2/0132/18. Forest Research received funding from the Forestry
758 Commission (climate change research programme). JCB acknowledges the support of Universidad Javeriana. JLBA received funding from
759 the Dirección General de Cambio Climático del Gobierno de Aragón; JLBA acknowledges fieldwork assistance by Ana Acín, the Ordesa y
760 Monte Perdido National Park, and the Servicio de Medio Ambiente de Soria de la Junta de Castilla y León. RGB and MPB received funding
761 from BECC - Biodiversity and Ecosystem services in a Changing Climate. MPB received funding from The European Union's Horizon 2020
762 research and innovation program under the Marie Skłodowska-Curie Grant Agreement No. 657627 and The Swedish Research Council
763 FORMAS – future research leaders No. 2016-01187. JB received funding from the Czech Academy of Sciences (grant nr. RVO 67985939).
764 NB received funding from the SNF (grant numbers 40FA40_154245, 20F121_148992, 20F120_173691, 407340_172433) and from the EU
765 (contract no. 774124). ICOS EU research infrastructure. EU FP7 NitroEurope. EU FP7 ECLAIRE. The authors from Biological Dynamics of
766 Forest Fragments Project, PDBFF, Instituto Nacional de Pesquisas da Amazônia, Brazil were supported by the MCTI/CNPq/FNDC – Ação
767 Transversal nº68/2013 – Programa de Grande Escala da Biosfera-Atmosfera na Amazônia – LBA; Project "Como as florestas da Amazônia
768 Central respondem às variações climáticas? Efeitos sobre dinâmica florestal e sinergia com a fragmentação florestal.". to The EUCLUX
769 Cooperative Research Program and Forest Science and Research Institute-IPEF. NC acknowledges funding by Stelvio National Park. JC was
770 funded by the Spanish government grant CGL2016-78093-R. ANID-FONDECYT 1181745 AND INSTITUTO ANTARTICO CHILENO (INACH FR-
771 0418). SC received funding from the German Research Foundation (grant no. DFG- FZT 118, 202548816). The National Science Foundation,
772 Poland (grant no. UMO-2017/27/B/ST10/02228), within the framework of the "Carbon dioxide uptake potential of sphagnum peatlands in
773 the context of atmospheric optical parameters and climate changes" (KUSCO2) project. SLC received funding from the South African
774 National Research Foundation and the Australian Research Council. FM, MČ, KU and MU received funding from Slovak Research and
775 Development Agency (no. APVV-19-0319). Instituto Antartico Chileno (INACH_RT-48_16), Iniciativa Científica Milenio Núcleo Milenio de
776 Salmónidos Invasores INVASAL, Institute of Ecology and Biodiversity (IEB), CONICYT PIA APOYO CCTE AFB170008. PC is supported by NERC
777 core funding to the BAS 'Biodiversity, Evolution and Adaptation Team. EJC received funding from the Norwegian Research Council (grant n
778 umber 230970). GND was supported by NERC E3 doctoral training partnership grant (NE/L002558/1) at the University of Edinburgh and
779 the Carnegie Trust for the Universities of Scotland. Monitoring stations on Livingston Island, Antarctica were funded by different research
780 projects of the Gobern of Spain (PERMAPLANET CTM2009-10165-E; ANTARPERMA CTM2011-15565-E; PERMASNOW CTM2014-52021-R),
781 and the PERMATHERMAL arrangement between the University of Alcalá and the Spanish Polar Committee. GN received funding from the
782 Autonomous Province of Bolzano (ITA). The infrastructure, part of the UK Environmental Change Network, was funded historically in part
783 by ScotNature and NERC National Capability LTS-S: UK-SCAPE; NE/R016429/1). JD was supported by the Czech Science Foundation
784 (GA17-19376S) and MSMT (LTAUSA18007). ED received funding from the Kempe Foundation (JCK-1112 and JCK-1822). The infrastructure
785 was supported by the Ministry of Education, Youth and Sports of the Czech Republic within the National Sustainability Programme I (NPU
786 I), grant number LO1415 and by the project for national infrastructure support CzeCOS/ICOS Reg.No. LM2015061. NE received funding
787 from the German Research Foundation (DFG- FZT 118, 202548816). BE received funding from the GLORIA-EU project no EVK2-CT2000-
788 00056, the Autonomous Province of Bolzano (ITA), from the Tiroler Wissenschaftsfonds and from the University of Innsbruck. RME was
789 supported by funding to the SAFE Project from the Sime Darby Foundation. OF received funding from the German Research Foundation
790 (DFG- FZT 118, 202548816). EFP was supported by the Jardín Botánico Atlántico (SV-20-GIJON-JBA). MF was funded by the German
791 Federal Ministry of Education and Research (BMBF) in the context of The Future Okavango (Grant No. 01LL0912) and SASSCAL
792 (01LG1201M; 01LG1201N) projects. RAG received funding from Fondecyt 11170516 and CONICYT PIA AFB170008. MBG received funding
793 from National Parks (DYNBIO, #1656/2015) and The Spanish Research Agency (VULBIMON, #CGL2017-90040-R). MG received funding from
794 the Swiss National Science Foundation (ICOS-CH Phase 2 20F120_173691). FG received funding from the German Research Foundation
795 (DFG- FZT 118, 202548816). KG and TS received funding from the UK Biotechnology and Biological Research Council (grant = 206/D16053).
796 SG was supported by the Research Foundation Flanders (FWO) (project G0H1517N). KJ and PH received funding from the EU Horizon2020
797 INFRAIA project eLTER-PLUS (871128), the project LTER-CWN (FFG, F&E Infrastrukturförderung, project number 858024) and the Austrian
798 Climate Research Program (ACRP7 – CentForCSink – KR14AC7K11960). SH and ARB received funding through iDiv funded by the German
799 Research Foundation (DFG- FZT 118, 202548816). LH received funding from the Czech Science Foundation (grant nr. 20-28119S) and the
800 Czech Academy of Sciences (grant nr. RVO 67985939). MH received funding from the Baden-Württemberg Ministry of Science, Research
801 and Arts via the project DRiE-R (Drought impacts, processes and resilience: making the in-visible visible). LH received funding from
802 International Polar Year, Weston Foundation, and ArcticNet. DH received funding from Natural Sciences and Engineering Council (Canada)
803 (RGPIN-06691). TTH received funding from Independent Research Fund Denmark (grant no. 8021-00423B) and Villum Foundation (grant
804 no. 17523). Ministry of Education, Youth and Sports of the Czech Republic (projects LM2015078, VAN2020/01 and
805 CZ.02.1.01/0.0/0.0/16_013/0001708). KH and CG received funding from Bolin Centre for Climate Research, Stockholm University and from
806 the Swedish research council Formas [grant n:o 2014-00530 to KH]. JJ received funding from the Funding Org. Swedish Forest Society
807 Foundation (grant nr. 2018-485-Steg 2 2017) and Swedish Research Council FORMAS (grant nr. 2018-00792). Project LAS III 77/2017/B
808 entitled: \"Estimation of net carbon dioxide fluxes exchanged between the forest ecosystem on post-agricultural land and between the
809 tornado-damaged forest area and the atmosphere using spectroscopic and numerical methods\", source of funding: General Directorate

810 of State Forests, Warsaw, Poland. AJ received funding from the German Federal Ministry of Education and Research BMBF (Grant Nr. FKZ
811 031B0516C SUSALPS) and the Oberfrankenstiftung (Grant Nr. OFS FP00237). ISJ received funding from the Energy Research Fund (NÝR-11 -
812 2019, NÝR-18 - 2020). TJ was supported by a UK NERC Independent Research Fellowship (grant number: NE/S01537X/1). RJ received
813 funding from National Science Centre of Poland (grant number: 2016/21/B/ST10/02271) and Polish National Centre for Research and
814 Development (grant number: Pol-Nor/203258/31/2013). VK received funding from the Czech Academy of Sciences (grant nr. RVO
815 67985939). AAK received funding from MoEFCC, Govt of India (AICOPTAX project F. No. 22018/12/2015/RE/Tax). NK received funding
816 from FORMAS, VR, support from the research infrastructure ICOS. BK received funding from the National Research, Development and
817 Innovation Fund of Hungary (grant nr. K128441). Ministry of Education, Youth and Sports of the Czech Republic (projects LM2015078 and
818 CZ.02.1.01/0.0/0.0/16_013/0001708). Project B1-RNM-163-UGR-18-Programa Operativo FEDER 2018, partially funded data collection.
819 Norwegian Research Council (NORKLIMA grants #184912 and #244525) awarded to Vigdís Vandvik. MM received funding from the Czech
820 Science Foundation (grant nr. 20-281195) and the Czech Academy of Sciences (grant nr. RVO 67985939). Project CONICYT-PAI 79170119
821 awarded to Roy Mackenzie. This work was partly funded by project MIUR PON Cluster OT4CLIMA. RM received funding from the SNF
822 project number 407340_172433. FM received funding from the Stelvio National Park. PM received funding from AIAS-COFUND fellowship
823 programme supported by the Marie Skłodowska-Curie actions under the European Union's Seventh Framework Programme for
824 Research, Technological development and Demonstration (grant agreement no 609033) and the Aarhus University Research Foundation,
825 Denmark. RM received funding from the Ministry of Education, Youth and Sports of the Czech Republic (project LTT17033). SM and VM
826 received funding from EU FP6 NitroEurope (grant nr. 17841), EU FP7 ÉCLAIRE (grant nr. 282910), the Ministry of Education and Science of
827 Ukraine (projects nr. 505, 550, 574, 602), GEF-UNEP funded "Toward INMS" project (grant nr. NEC05348) and ENI CBC BSB PONTOS (grant
828 nr. BSB 889). STM received funding from New Frontiers in Research Fund-Exploration (grant nr. NFRF-2018-02043) and NSERC Discovery.
829 MMR received funding from the Australian Research Council Discovery Early Career Research Award (grant nr. DE180100570). JAM
830 received funding from the National Science Foundation (DEB 1557094), International Center for Advanced Renewable Energy and
831 Sustainability (I-CARES) at Washington University in St. Louis, ForestGEO, and Tyson Research Center. IM-S was funded by the UK Natural
832 Environment Research Council through the ShrubTundra Project (NE/M016323/1). MBN received funding from FORMAS, VR, Kempe
833 Foundations support from the research infrastructures ICOS and SITES. MDN received funding from CONICET (grant nr. PIP 112-201501-
834 00609). Spanish Ministry of Science grant PID2019-110521GB-I00 and Catalan government grant 2017-1005. French National Research
835 Agency (ANR) in the frame of the Cluster of Excellence COTE (project HydroBeech, ANR-10-LABX-45). VLIR-OUS, under the Institutional
836 University Cooperation programme (IUC) with Mountains of the Moon University, Max Planck Society (Germany), RFBR, Krasnoyarsk
837 Territory and Krasnoyarsk Regional Fund of Science, project number 20-45-242908. Estonian Research Council (PRG609), and the
838 European Regional Development Fund (Centre of Excellence EcoChange). Canada-Denmark Arctic Research Station Early Career Scientist
839 Exchange Program, from Polar knowledge Canada (POLAR) and the Danish Agency for Science and Higher Education. Fondecyt 1180205
840 and CONICYT PIA AFB170008. MP received funding from the Funding Org. Knut and Alice Wallenberg Foundation (grant nr. 2015.0047),
841 and acknowledges funding from the Swedish Research Council (VR) with contributing research institutes to both the SITES and ICOS
842 Sweden infrastructures. Spanish Ministry of Science grant PID2019-110521GB-I00, fundación Ramón Areces ELEMENTAL-CLIMATE project,
843 and Catalan government grant 2017-1005. MPB received funding from the Svalbard Environmental Protection Fund (grant project number
844 15/128) and the Research Council of Norway (Arctic Field Grant, project number 269957). RP received funding from the Ministry of
845 Education, Youth and Sports of the Czech Republic (grant INTER-TRANSFER nr. LTT20017). LTSER Zone Atelier Alpes; Fédération FREE-
846 Alpes. RP received funding from a Humboldt Fellowship for Experienced Researchers. RPU received funding from the Polish National
847 Science Centre (grant project number 2017/27/B/NZ8/00316). ODYSSEE project (ANR-13-ISV7-0004, PN-II-ID-JRP-RO-FR-2012). KR was
848 supported through an Australian Government Research Training Program Scholarship. Fieldwork was supported by the Global Challenges
849 program at the University of Wollongong, the ARC the Australian Antarctic Division and INACH. Project SUBANTECO IPEV 136 (French Polar
850 Institute Paul-Emile Victor), Zone Atelier CNRS Antarctique et Terres Australes, SAD Région Bretagne (Project INFILCT), BiodivERsA 2019-
851 2020 BioDivClim call 'ASICS' (ANR-20-EBI5-0004). SAR received funding from the Australian Research Council. NSF grant #1556772 to the
852 University of Notre Dame. Pavia University (Italy). OR received funding from EU-LEAP-Agri (RAMSES II), EU-DESIRA (CASSECS), EU-H2020
853 (SustainSahel), AGROPOLIS and TOTAL Foundations (DSCATT), CGIAR (GLDC). AR was supported by the Russian Science Foundation (Grant
854 18-74-10048). Parc national des Ecrins. JS received funding from Vetenskapsrådet grant nr (No: 2014-04270), ALTER-net multi site grant,
855 River LIFE project (LIFE08 NAT/S/000266), Flexpeil. Helmholtz Association long-term research program TERENO (Terrestrial Environmental
856 Observatories). PS received funding from the Polish Ministry of Science and Higher Education (grant nr. N N305 304840). AS received
857 funding from the ETH Research grant (grant number ETH-27 19-1). LSC received funding from NSERC Canada Graduate Scholarship
858 (Doctoral) Program; LSC was also supported by ArcticNet-NCE. Conselho Nacional de Desenvolvimento Científico e Tecnológico
859 (141513/2017-9); Fundação Carlos Chagas Filho de Amparo à Pesquisa do Estado do Rio de Janeiro (E26/200.84/2019). ZS received funding
860 from the SRDA (nr. APVV-16-0325) and from the ERDF (grant nr. ITMS 313011S735, CE LignoSilva). JS, MB, and CA received funding from
861 core budget of ETH Zurich. State excellence Program M-V \"WETSCAPES\". AfricanBioServices project funded by the EU Horizon 2020 grant
862 number 641918. The authors from KIT/IMK-IFU acknowledge the funding received within the German Terrestrial Environmental
863 Observatories (TERENO) research program of the Helmholtz Association and from the Bavarian Ministry of the Environment and Public
864 Health (UGV06080204000). Deutsche Forschungsgemeinschaft (DFG, German Research Foundation), project number 192626868, in the
865 framework of the collaborative German-Indonesian research project CRC 990 (SFB): \"EFForTS, Ecological and Socioeconomic Functions of
866 Tropical Lowland Rainforest Transformation Systems (Sumatra, Indonesia)\". MS received funding from the Ministry of Education, Youth
867 and Sports of the Czech Republic (grant nr. INTER-TRANSFER LTT19018). TT received funding from the Swedish National Space Board (SNSB
868 Dnr 95/16) and the CASSECS project supported by the European Union. HJDT received funding from the UK Natural Environment Research
869 Council (NERC doctoral training partnership grant NE/L002558/1). German Science Foundation (DFG) GraKo 2010 \"Response\". PDT
870 received funding from the MEMOIRE project (PN-III-P1-1.1-PD2016-0925). Arctic Challenge for Sustainability II (ArCS II;
871 JPMXD1420318865). JU received funding from Czech Science Foundation (grant nr. 21-11487S). TU received funding from the Romanian
872 Ministry of Education and Research (CCCDI - UEFISCDI -project PN-III-P2-2.1-PED-2019-4924 and PN2019-2022/19270201-Ctr. 25N
873 BIODIVERS 3-BIOSERV). LvDB, KT, MYB and RC acknowledge funding from the German Research Foundation within the Priority Program
874 SPP-1803 \"EarthShape: Earth Surface Shaping by Biota\" (grant TI 338/14-1&2 and BA 3843/6-1). AV acknowledge funding from RSF,
875 project 21-14-00209. GFV received funding from the Dutch Research Council NWO (Veni grant, no. 863.14.013). Australian Research

876 Council Discovery Early Career Research Award DE140101611. FGAV received funding from the Portuguese Science Foundation (FCT)
877 under CEECIND/02509/2018, CESAM (UIDP/50017/2020+UIDB/50017/2020), FCT/MCTES through national funds, and the co-funding by
878 the FEDER, within the PT2020 Partnership Agreement and Compete 2020. Ordesa y Monte Perdido National Park. MVI received funding
879 from the Spanish Ministry of Science and Innovation through a doctoral grant (FPU17/05869). JW received funding from the Czech Science
880 Foundation (grant nr. 20-28119S) and the Czech Academy of Sciences (grant nr. RVO 67985939). CR and SW received funding from the
881 Swiss Federal Office for the Environment (FOEN) and the de Giacomi foundation. YY received funding from the National Natural Science
882 Foundation of China (Grant no. 41861134039 and 41941015). ZY received funding from the National Natural Science Foundation of China
883 (grant nr. 41877458). FZ received funding from the Swiss National Science Foundation (grant nr. 172198 and 193645). PZ received funding
884 from the Funding Org. Knut and Alice Wallenberg Foundation (grant no. 2015.0047). JL received funding from: (i) the Agence Nationale de
885 la Recherche (ANR), under the framework of the young investigators (JCJC) funding instrument (ANR JCJC Grant project N°ANR-19-CE32-
886 0005-01: IMPRINT); (ii) the Centre National de la Recherche Scientifique (CNRS) (Défi INFINITI 2018: MORFO); and the Structure Fédérative
887 de Recherche (SFR) Condorcet (FR CNRS 3417: CREUSE).

888 Fieldwork in the Arctic got facilitated by funding from the EU INTERACT program. SN, UAT, JJA, and JvO would like to thank the field team
889 of the Vegetation Dynamics group for their efforts and hard work. We acknowledge Dominique Tristan for letting access to the field. for
890 the logistic support the crew of INACH and Gabriel de Castilla Station team on Deception Island. We thank the Inuvialuit and Kluane First
891 Nations for the opportunity to work on their land. MAdP acknowledges fieldwork assistance and logistics support to Unidad de Tecnología
892 Marina CSIC, and the crew of Juan Carlos I and Gabriel de Castilla Spanish Antarctic Stations, as well as to the different colleagues from
893 UAH that helped on the instruments maintainance. ERF acknowledges fieldwork assistance by Martin Heggli. MBG acknowledges fieldwork
894 and technical assistance by P Abadía, C Benedé, P Bravo, J Gómez, M Grasa, R Jimenez, H Miranda, B Ponz, J Revilla and P Tejero, and the
895 Ordesa and Monte Perdido National Park staff. LH acknowledges field assistance by John Jacobs, Andrew Trant, Robert Way, Darroch
896 Whitaker; I acknowledge the Inuit of Nunatsiavut, and the Cooperative Management Board of Torngat Mountains National Park for their
897 support of this project and acknowledge that the field research was conducted on their traditional lands. We thank our many bear guides,
898 especially Boonie, Eli, Herman, John, and Maria Merkuratsuk. AAK acknowledges field support of Akhtar Malik, Rameez Ahmad. Part of
899 microclimatic records from Saxony was funded by the Saxon Switzerland National Park Administration. Tyson Research Center. JP
900 acknowledges field support of Emmanuel Malet (Edytem) and Rangers of Reserves Naturelles de Haute-Savoie (ASTERS). practical help:
901 Roel H. Janssen, N. Huig, E. Bakker, Schools in the tepåseförsöket, Forskar fredag, Erik Herberg. The support by the Bavarian Forest
902 National Park administration is highly appreciated. Liesbeth acknowledges CONAF and onsite support from the park rangers from PN Pan
903 de Azucar, PN La Campana, PN Nahuelbuta and from comunidad agricola Quebrada de Talca. JL and FS acknowledge Manuel Nicolas and
904 all forest officers from the Office National des Forêts (ONF) who are in charge of the RENECOFOR network and who provided help and
905 local support for the installation and maintenance of temperature loggers in the field.

906 **Author contributions**

907 JJL and JL conceptualized the project, JJL, JvdH, MBA, PDF, MK, ML, IMDM, TWC, IN and JL designed
908 the paper, the SoilTemp consortium acquired the data, JJL, JVDH, JK, and PN analysed the data, JJL,
909 JvdH, JA, MBA, PDF, JK, MK, ML, IMDM, TWC, JJB, SH, DHK, PN, BRS and KVM interpreted the
910 analyses. All authors significantly revised the manuscript and approved it for submission.

911 **The authors declare no competing interests.**

912 **Affiliations**

913 1) Research Group PLECO (Plants and Ecosystems), University of Antwerp, 2610 Wilrijk, Belgium, 2) Department of Environmental Systems
914 Science, Institute of Integrative Biology, ETH Zürich, Zürich, Switzerland, 3) Finnish Meteorological Inst., P.O. Box 503, FI-00101 Helsinki,
915 Finland, 4) Dept of Geosciences and Geography, Gustaf Hällströmin katu 2a, FIN-00014 Univ. of Helsinki, Finland, 5) Centre for Sustainable
916 Ecosystem Solutions, School of Earth, Atmospheric and Life Sciences, University of Wollongong, Wollongong, New South Wales, 2522,
917 Australia, 6) Australian Museum, Sydney, Australia, 7) Forest & Nature Lab, Department of Environment, Ghent University,
918 Geraardsbergensesteenweg 267, 9090 Melle-Gontrode, Belgium, 8) Geography Research Unit, University of Oulu, Oulu, Finland, 9) Institute
919 of Botany of the Czech Academy of Sciences, Zámek 1, CZ-25243, Průhonice, Czech Republic, 10) Faculty of Forestry and Wood Sciences,
920 Czech University of Life Sciences Prague, Kamýcká 129, CZ-165 21, Prague 6 - Suchdol, Czech Republic, 11) Environment and Sustainability
921 Institute, University of Exeter, Penryn Campus, Penryn, UK, TR10 9FE, 12) Department of Geography, York St John University, Lord Mayor's
922 Walk, York, YO31 7EX, United Kingdom, 13) Department of Earth and Environmental Sciences, KU Leuven, Celestijnenlaan 200E, 3001
923 Leuven, Belgium, 14) School of Natural Resources and Environment, University of Florida, Gainesville, FL 32611, USA, 15) Smithsonian
924 Environmental Research Center, Edgewater MD 21037 USA, 16) Department of Wildlife Ecology and Conservation, University of Florida,
925 Gainesville, FL 32611, USA, 17) Department of Natural Sciences and Environmental Health, University of South-Eastern Norway,
926 Gullbringvegen 36, NO-3800, Bø, Norway, 18) Alpine Ecosystems Research Program, Institute of Ecology, Ilia State University, Tbilisi,
927 Georgia, 19) Department of Range Management, Faculty of Natural Resources and Marine Sciences, Tarbiat Modares University, Noor,
928 Mazandaran Province, I. R. Iran, 20) Department of Ecological Science, Vrije Universiteit Amsterdam, The Netherlands., 21) Royal Botanic
929 Garden Edinburgh, 20A Inverleith Row, EH3 5LR, Edinburgh, UK, 22) Environmental Science Center, Qatar University, Doha, Qatar, 23)
930 Department of Environmental Systems Science, Institute of Integrative Biology, ETH Zurich, Universitätsstrasse 16, CH-8092 Zürich,
931 Switzerland, 24) Research group ECOBE, University of Antwerp, 2610 Wilrijk, Belgium, 25) Department of Agroecology and Environment,
932 Agroscope Research Institute, Reckenholzstrasse 191, 8046 Zürich, Switzerland, 26) Department of Environmental Systems Science, ETH
933 Zurich, Universitaetstrasse 2, 8092 Zurich, Switzerland, 27) UK Centre for Ecology & Hydrology, Bush Estate, Penicuik, Midlothian, EH26

934 0QB, United Kingdom, 28) Department of Physical Geography and Ecosystem Science, Lund University, Sölvegatan 12, 223 62 Lund,
935 Sweden, 29) European Commission, Joint Research Centre (JRC), Ispra, Italy, 30) Siberian Federal University, 660041 Krasnoyarsk, Russia,
936 31) Instituto Argentino de Nivología, Glaciología y Ciencias Ambientales (IANIGLA), CONICET, CCT-Mendoza; Facultad de Ciencias Exactas y
937 Naturales, Universidad Nacional de Cuyo, 32) Instituto Argentino de Nivología, Glaciología y Ciencias Ambientales (IANIGLA), CONICET,
938 CCT-Mendoza, 33) Natural History Museum, University of Oslo, 0318, Oslo, Norway, 34) Section for Ecoinformatics & Biodiversity,
939 Department of Biology, Aarhus University, Aarhus C, Denmark, 35) Center for Biodiversity Dynamics in a Changing World, Department of
940 Biology, Aarhus University, Aarhus C, Denmark, 36) Ecological Plant Geography, Faculty of Geography, University of Marburg,
941 Deutschhausstrasse 10, 35032, Marburg, Germany, 37) Institute of Landscape Ecology Slovak Academy of Sciences, Štefánikova 3, 81499
942 Bratislava, Slovakia, 38) Faculty of Environmental and Forest Sciences, Agricultural University of Iceland, Árleyni 22, 112 Reykjavík, Iceland,
943 39) Instituto Argentino de Nivología, Glaciología y Ciencias Ambientales (IANIGLA), CONICET, CCT-Mendoza, 40) Isotope Bioscience
944 Laboratory - ISOFYS, Ghent University, Coupure Links 653, 9000 Gent, Belgium, 41) Université de Rennes, CNRS, EcoBio (Ecosystèmes,
945 biodiversité, évolution) - UMR 6553, F-35000 Rennes, France, 42) Department of Sustainable Agro-ecosystems and Bioresources, Research
946 and Innovation Centre, Fondazione Edmund Mach, Via E. Mach 1, 38010 San Michele all'Adige, Italy, 43) Forest Research, Alice Holt Lodge,
947 Wrecclesham, Farnham, UK, 44) Department of Ecology, Pontificia Universidad Javeriana, Bogota, Colombia, 45) Jolube Consultor
948 Botánico. C/Mariano R de Ledesma, 4. E-22700 Jaca, Huesca, SPAIN, 46) Institute of Landscape and Plant Ecology, Department of Plant
949 Ecology, University of Hohenheim, Otilie-Zeller_weg 2, 70599 Stuttgart, Germany, 47) Disturbance Ecology, BayCEER, University of
950 Bayreuth, Universitätsstr. 30, 95447 Bayreuth, Germany, 48) Norwegian Institute for Nature Research, FRAM - High North Research Centre
951 for Climate and the Environment, P.O. Box 6606 Langnes, N-9296 Tromsø, Norway, 49) Department of Earth Sciences, University of
952 Gothenburg, P.O. Box 460, SE-40530 Gothenburg, Sweden, 50) Gothenburg Global Biodiversity Centre, P.O. Box 461, SE-405 30
953 Gothenburg, Sweden, 51) Department of Biological and Environmental Sciences, University of Gothenburg, P.O. Box 461, 43 Gothenburg
954 SE-405 30, Sweden, 52) Department of Environmental Science, Policy, and Management, University of California, Berkeley, CA 94720 USA,
955 53) Alfred Wegener Institute Helmholtz Center for Polar and Marine Research, Telegrafenberg A45, 14473 Potsdam, Germany, 54)
956 Geography Department, Humboldt-Universität zu Berlin, Germany, 55) Pós-Graduação em Ciências de Florestas Tropicais, Instituto
957 Nacional de Pesquisas da Amazônia, Manaus, Brasil, CEP: 69060-001, 56) UMR ECOSYS INRAE, AgroParisTech, Uinversité Paris Saclay,
958 France, 57) Biological Dynamics of Forest Fragments Project, BDFFP, Instituto Nacional de Pesquisas da Amazônia, Av. André Araujo, 2936 -
959 Petrópolis, Manaus, Amazonas, 69067-375, Brazil, 58) Department of Forest Sciences, Federal University of Lavras, 37.200-900, Lavras,
960 MG, Brazil, 59) Faculty of Arts and Sciences, Department of Molecular Biology and Genetics, Ordu University, 52200, Ordu, Turkey, 60)
961 Ecological Plant Geography, Faculty of Geography, University of Marburg, Deutschhausstrasse 10, 35032, Marburg, Germany., 61) Plant
962 Ecology Group, Department of Evolution and Ecology, University of Tübingen, Auf der Morgenstelle 5, 72076 Tübingen, Germany, 62)
963 Department of Science and High Technology, Insubria University, Via Valleggio 11, 22100 Como, Italy, 63) Department of Chemistry, Life
964 Sciences and Environmental Sustainability, University of Parma, Parco Area delle Scienze 11/A, 43124 Parma, Italy, 64) Department of
965 Evolutionary Biology, Ecology and Environmental Sciences, Biodiversity Research Institute (IRBio), University of Barcelona, 08028
966 Barcelona, Catalonia, Spain, 65) CREAF, E08193 Bellaterra (Cerdanyola del Vallès), Catalonia, Spain, 66) Laboratorio de Ecofisiología vegetal
967 y Cambio Climático and Núcleo de Estudios Ambientales (NEA), Universidad Católica de Temuco, Campus Luis Rivas del Canto, Rudecindo
968 Ortega 02950, Temuco, Chile., 67) German Centre for Integrative Biodiversity Research (iDiv) Halle-Jena-Leipzig, Leipzig, Germany, 68)
969 Institute of Biology, Leipzig University, Leipzig, Germany, 69) Laboratory of Bioclimatology, Department of Ecology and Environmental
970 Protection, Poznan University of Life Sciences, ul. Piątkowska 94, 60-649, Poznan, Poland, 70) Univ. Grenoble Alpes, Univ. Savoie Mont
971 Blanc, CNRS, LECA, F-38000 Grenoble, France, 71) Univ. Grenoble Alpes, Univ. Savoie Mont Blanc, CNRS, LTSER Zone Atelier Alpes, F-38000
972 Grenoble, France, 72) Securing Antarctica's Environmental Future, School of Biological Sciences, Monash University, Victoria 3800,
973 Australia, 73) Forest Ecology and Conservation Group, Department of Plant Sciences, University of Cambridge, Cambridge CB23EA, UK, 74)
974 Faculty of Ecology and Environmental Sciences, Technical University in Zvolen, T. G. Masaryka 24, 960 01 Zvolen, Slovakia, 75) Sub-
975 Antarctic Biocultural Conservation Program, Universidad de Magallanes, Pdte. Manuel Bulnes 01855, Punta Arenas, Magallanes y la
976 Antártica Chilena, 76) Núcleo Milenio de Salmónidos Invasores, INVASAL, Concepción, Chile, 77) British Antarctic Survey, NERC, High Cross,
977 Madingley Road, Cambridge CB3 0ET, United Kingdom, 78) Department of Arctic and Marine Biology, Faculty of Biosciences Fisheries and
978 Economics, UiT-The Arctic University of Norway, N-9037 Tromsø, Norway, 79) Climate Change Unit, Environmental Protection Agency of
979 Aosta Valley, Italy, 80) Department of Biological Sciences, University of Notre Dame, Notre Dame, IN 46556, USA, 81) Department of
980 Science, University of Roma Tre, 00146 Rome, Italy, 82) Department of Ecology, Environment and Plant Sciences and Bolin Centre for
981 Climate Research, Stockholm University, 106 91 Stockholm, Sweden, 83) the County Administrative Board of Västra Götaland, SE-403 40
982 Gothenburg, Sweden, 84) School of GeoSciences, University of Edinburgh, King's Buildings, Edinburgh, EH9 3FF, United Kingdom, 85)
983 Department of Geology, Geography and Environment. University of Alcalá. 28805 Alcalá de Henares, Madrid, Spain., 86) Chair of
984 Geoinformatics, Technische Universität Dresden, Dresden Germany, 87) Vegetation Ecology, Institute of Natural Resource Sciences, ZHAW
985 Zurich University of Applied Sciences, Grüental, 8820 Wädenswil, Switzerland, 88) Plant Ecology, Bayreuth Center of Ecology and
986 Environmental Research (BayCEER), University of Bayreuth, Universitätsstr. 30, 95447 Bayreuth, Germany, 89) VITO-TAP, Boeretang 200,
987 2400-Mol, Belgium, 90) Swiss Federal Research Institute WSL, 8903 Birmensdorf, Switzerland, 91) Majella Seed Bank, Majella National
988 Park, Colle Madonna, 66010 Lama dei Peligni, Italy, 92) Department of Life, Health and Environmental Sciences, University of L'Aquila,
989 Piazzale Salvatore Tommasi 1, 67100 L'Aquila, Italy, 93) Grupo de Ecología de Poblaciones de Insectos, IFAB (INTA - CONICET), Modesta
990 Victoria 4450, Bariloche, Argentina, 94) Department of Biology and Biochemistry, University of Houston, Houston, Texas, 77204 USA, 95)
991 Faculty of Science, Department of Botany, University of South Bohemia, Na Zlaté Stoce 1, 37005 České Budějovice, Czech Republic, 96)
992 Climate Impacts Research Centre, Department of Ecology and Environmental Sciences, Umeå University, Abisko, Sweden, 97) Global
993 Change Research Institute, Academy of Sciences of the Czech Republic, 98) Department of Ecology & Evolutionary Biology, University of
994 Arizona, USA, 99) School of Biological Sciences, The University of Western Australia, Crawley, WA 6009, Australia, 100) Kings Park Science,
995 Department of Biodiversity, Conservation & Attractions, Kings Park, 6005 WA, Australia, 101) Department of Botany, Faculty of Biology,
996 University of Innsbruck, Sternwartestraße 15, 6020 Innsbruck, Austria, 102) Imperial College London, Silwood Park Campus, Ascot SL5 7PY,
997 UK, 103) Operation Wallacea, Wallace House, Old Bolingbroke, Lincolnshire, PE23 4EX, UK, 104) INRAE, Bordeaux Sciences Agro, UMR
998 1391 ISPA, F-33140 Villenave d'Ornon, France, 105) Department of Life and Environmental Sciences, University of Cagliari, Viale
999 Sant'Ignazio da Laconi 13, 09123, Cagliari, Italy., 106) Department of Botany, University of Granada, 18071, Granada, Spain, 107) IMIB –

1000 Biodiversity Research Institute, University of Oviedo, Mieres, Spain, 108) Institute for Plant Science and Microbiology, University of
1001 Hamburg, Ohnhorststr. 18, 22609 Hamburg, Germany, 109) Dartmouth College, Hanover, NH, USA, 110) Ecosystems and Global Change
1002 Group, Department of Plant Sciences, University of Cambridge, Cambridge, CB2 3EA, United Kingdom, 111) WSL Institute for Snow and
1003 Avalanche Research SLF, 7260 Davos, Switzerland, 112) Swiss Federal Research Institute for Forest, Snow and Landscape Research WSL,
1004 8903 Birmensdorf, Switzerland, 113) Laboratorio de Invasiones Biológicas (LIB), Facultad de Ciencias Forestales, Universidad de
1005 Concepción, Concepción, Chile, 114) School of Education and Social Sciences, Adventist University of Chile, Chile, 115) Instituto de Ecología
1006 y Biodiversidad (IEB), Santiago, Chile, 116) Pyrenean Institute of Ecology (CSIC), Av. Montañana 1005, 50059 Zaragoza, Spain, 117)
1007 Biodiversity and Landscape, TERRA research centre, Gembloux Agro-Bio Tech, University of Liège, Gembloux, 5032, Belgium ; Research
1008 Group PLECO (Plants and Ecosystems), University of Antwerp, 2610 Wilrijk, Belgium, 118) Department of Geo-information in
1009 Environmental Management, Mediterranean Agronomic Institute of Chania, PO Box 85, 73100 Chania, Greece, 119) Georgian Institute of
1010 Public Affairs, department of Environmental management ad policy, Tbilisi, Georgia, 120) Flemish Institute for Technological Research,
1011 2400 Mol, Belgium, 121) Department of Earth and Environmental Science, Faculty of BioScience Engineering, KULeuven, Belgium, 122)
1012 Max Planck Institute for Biogeochemistry, Department of Biogeochemical Signals, Jena, Germany, 123) Sustainable Agricultural Sciences
1013 Department, Rothamsted Research, Harpenden, AL5 2JQ, UK, 124) Department of Biology, Norwegian University of Science and
1014 Technology, 7491 Trondheim, Norway, 125) Biodiversity, Wildlife and Ecosystem Health, Biomedical Sciences, University of Edinburgh,
1015 Edinburgh, EH8 9JZ, UK, 126) Department of Ecology, Swedish University of Agricultural Sciences, Box 7042, S-750 07 Uppsala, 127) School
1016 of Biological Sciences, The University of Hong Kong, Pok Fu Lam Road, Hong Kong SAR, China, 128) Department of Theoretical and Applied
1017 Sciences, Insubria University, Via Dunant 3, 21100 Varese, Italy, 129) CIRAD, UMR Eco&Sols, 34060 Montpellier, France, 130) Eco&Sols,
1018 Univ Montpellier, CIRAD, INRAE, IRD, Montpellier SupAgro, 34060 Montpellier, France, 131) Senckenberg Research Institute and Natural
1019 History Museum Frankfurt, 63571 Gelnhausen, Germany, 132) Faculty of Biology, University of Duisburg-Essen, 45141 Essen, Germany,
1020 133) Institute of Biology / Geobotany and Botanical Garden, Martin Luther University Halle-Wittenberg, Halle (Saale), Germany, 134)
1021 Department of Biological Sciences and Bjerknes Centre for Climate Research, University of Bergen, N-5020 Bergen, Norway, 135) Centre
1022 for Biodiversity & Taxonomy, Department of Botany, University of Kashmir, Srinagar - 190006, J&K, India, 136) Department of Ecology,
1023 University of Innsbruck, 6020 Innsbruck, Austria, 137) INRAE, Univ. Bordeaux, BIOGECO, F-33610 Cestas, France, 138) Museumsenteret i
1024 Hordaland, Lyngheisenteret, Alver, Norway, 139) TERRA Teaching and Research Center, Faculty of Gembloux Agro-Bio Tech, University of
1025 Liege, Passage des déportés, 2, 5030 Gembloux, Belgium, 140) UK Centre for Ecology & Hydrology, Penicuik, EH26 0QB, Scotland, UK., 141)
1026 Institute for Botany, University of Natural Resources and Life Sciences Vienna (BOKU), Gregor-Mendel-Straße 33/I, 1180 Vienna, Austria,
1027 142) Centre for Agrometeorological Research (ZAMF), German Meteorological Service (DWD), Bundesallee 33, 38116 Braunschweig,
1028 Germany, 143) Dept of Biology, Memorial University, St. John's, NL, A1B 3X9. Canada, 144) Department of Biological Sciences, Simon
1029 Fraser University, Burnaby, BC, V5A 1S6, Canada, 145) Department of Geography, University of Zaragoza, Pedro Cerbuna 12, 50009
1030 Zaragoza, Spain, 146) Plant Ecology, Albrecht-von-Haller-Institute for Plant Sciences, Georg-August University of Goettingen, Untere
1031 Karspuele 2, 37073 Goettingen, Germany, 147) Department of Bioscience and Arctic Research Centre, Aarhus University, Grenåvej 14,
1032 8410 Rønde, Denmark, 148) Department of Geography, Masaryk University, Faculty of Science, Kotlarska 2, 611 37, Brno, Czech Republic,
1033 149) Department of Environmental Science, Shinshu University, Matsumoto, Japan, 150) Department of Bioscience and Arctic Research
1034 Centre, Aarhus University, Frederiksborgvej 399, 4000 Roskilde, Denmark, 151) INRAE, University of Bordeaux, BIOGECO, F-33610 Cestas,
1035 France, 152) Department of Forest Ecology and Management, Swedish University of Agricultural Sciences, 90183 Umeå, Sweden, 153)
1036 Laboratory of Meteorology, Department of Construction and Geoengineering, Faculty of Environmental Engineering and Mechanical
1037 Engineering, Poznan University of Life Sciences, ul. Piątkowska 94, 60-649, Poznan, Poland, 154) Forest Research Institute, Department of
1038 Silviculture and Forest Tree Genetics, Braci Lesnej Street, No 3, Sekocin Stary, 05-090 Raszyn, Poland, 155) Bayreuth Center of Ecology and
1039 Environmental Research, 156) ARAID/IPE-CSIC, Pyrenean Institute of Ecology, Avda. Llano de la Victoria, 16, Jaca 22700, Spain, 157) Life
1040 and Environmental Sciences, University of Iceland, Sturlugata 7, 102 Reykjavík, Iceland, 158) Soil Science Department, Federal University of
1041 Viçosa, Prof. Peter Henry Rolfs Ave., 36570-900, Viçosa-MG, Brazil, 159) School of Biological Sciences, University of Bristol, Bristol, United
1042 Kingdom, 160) Biological and Environmental Sciences, Faculty of Natural Sciences, University of Stirling, Scotland, FK9 4LA, 161) Faculty of
1043 Environmental Sciences, Czech University of Life Sciences Prague, Kamýcká 129, 165 21 Prague 6 - Suchdol, Czech Republic, 162) Centre for
1044 Environmental and Climate Science, Lund University, Sölvegatan 37, 223 62, Lund, Sweden, 163) University of Goettingen, Bioclimatology,
1045 Büsgenweg 2, 37077 Göttingen, Germany., 164) Environment Agency Austria, Spittelauer Lände 5, 1090 Vienna, Austria, 165) Max Planck
1046 Institute for Biogeochemistry, Jena, Thuringia, Germany, 166) Centre for Ecological Research, Institute of Ecology and Botany, H-2163
1047 Vácrátót, Alkotmány út 2-4., Hungary, 167) Experimental Plant Ecology, Institute of Botany and Landscape Ecology, University of
1048 Greifswald, D-17487 Greifswald, Germany, 168) GLORIA Coordination, Institute for Interdisciplinary Mountain Research, Austrian Academy
1049 of Sciences (ÖAW) & Department of Integrative Biology and Biodiversity Research, University of Natural Resources and Life Sciences,
1050 Vienna (BOKU), Silbergasse 30/3, 1190 Vienna, Austria, 169) Department of Arctic Biology, The University Centre in Svalbard (UNIS), 9171
1051 Longyearbyen, Svalbard, Norway, 170) Department of Land Resources and Environmental Sciences, Montana State University, Bozeman
1052 MT, USA, 59717, 171) Climate Impacts Research Centre, Department of Ecology and Environmental Sciences, Umeå University,
1053 Vetenskapens väg 38, 98107 Abisko, Sweden, 172) Centre for Polar Ecology, Faculty of Science, University of South Bohemia, Na Zlaté
1054 Stoce 3, CZ-370 05, České Budějovice, Czech Republic, 173) School of Biological Sciences, Monash University, Victoria 3800, Australia, 174)
1055 Terrestrial Ecology Unit, Dept. of Biology, Ghent University, B-9000 Gent, Belgium, 175) Finnish Meteorological Institute, Climate System
1056 Research, PoB503, 00101 Helsinki, Finland, 176) INAR Institute for Atmospheric and Earth System Research/Physics, Faculty of Science,
1057 POBox 68 FI-00014 University of Helsinki, Finland, 177) Interuniversity Institute for Earth System Research, University of Granada, Granada
1058 18006 Spain, 178) CNR Institute for Agricultural and Forestry Systems in the Mediterranean, P.le Enrico Fermi 1 - Loc. del Granatello,
1059 80055, Portici (Napoli) Italy, 179) Faculty of Forestry, Technical University in Zvolen, T.G.Masaryka 24, 960 01 Zvolen, Slovakia, 180) CNR
1060 Institute for Agricultural and Forestry Systems in the Mediterranean, P.le Enrico Fermi 1 - Loc. del Granatello, 80055, Portici (Napoli) Italy,
1061 181) School of Pure & Applied Sciences, Environmental Conservation & Management Programme Open University of Cyprus, PO Box
1062 12794, 2252 Latsia, Nicosia, 182) Department of Biology - Aquatic Biology, Aarhus University, Ole Worms Allé 1, 8000 Aarhus C, Denmark,
1063 183) Aarhus Institute of Advanced Studies, AIAS Høegh-Guldbergs Gade 6B, 8000 Aarhus, Denmark, 184) CNR Institute of BioEconomy, Via
1064 Gobetti 101, 40129 Bologna, Italy, 185) Department of Forest Botany, Dendrology and Geobiocoenology, Faculty of Forestry and Wood
1065 Technology, Mendel University in Brno, Zemedelska 1, 613 00 Brno, Czech Republic, 186) Regional Centre for Integrated Environmental

1066 Monitoring, Odesa National I.I. Mechnikov University, 7 Mayakovskogo lane, 65082 Odesa, Ukraine, 187) Department of Agroecology,
1067 Aarhus University, 20 Blichers Allé, 8830 Tjele, Denmark, 188) NGO New Energy, 11 Bakulina str., 61166 Kharkiv, Ukraine, 189) Biological
1068 Dynamics of Forest Fragments Project, Coordenação de Dinâmica Ambiental, Instituto Nacional de Pesquisas da Amazônia, Manaus, AM
1069 CEP 69067-375, Brazil., 190) Swiss Federal Institute for Forest, Snow and Landscape Research (WSL), CH-8903 Birmensdorf, Switzerland.,
1070 191) Department of Biology, University of Antwerp, Universiteitsplein 1, 2610 Wilrijk, Belgium, 192) Department of Botany and
1071 Biodiversity Research Centre, University of British Columbia, Vancouver, BC, Canada, 193) Province of Antwerp, Koningin Elisabethlei 22,
1072 2018 Antwerpen, Belgium, 194) Institute of Plant and Animal Ecology of Ural Division of Russian Academy of Science, 8 Marta st., 202,
1073 Ekaterinburg, Russia, 195) Department of Earth and Environmental Sciences, University of Pavia, Via S. Epifanio 14, Pavia, Italy, 196)
1074 Faculty of Science and Technology, Free University of Bolzano, Piazza Università 5, 39100 Bolzano, Italy, 197) Climate Change Unit,
1075 Environmental Protection Agency of Aosta Valley, Loc. La Maladière, 48, 11020 Saint-Christophe, Italy, 198) University of Freiburg, Chair of
1076 Geobotany, Schänzlestrasse 1, 79104 Freiburg, Germany, 199) Environment and Sustainability Institute, University of Exeter, Penryn
1077 Campus, Cornwall TR10 9FE, United Kingdom, 200) Centre for Ecosystem Science, School of Biological, Earth and Environmental Sciences,
1078 UNSW Sydney, NSW 2052, Sydney, Australia, 201) Department of Biology, Washington University in St. Louis, St. Louis, MO 63130, USA.,
1079 202) Department of Animal Biology, Institute of Biology, University of Campinas, Campinas, SP, CEP 13083-862, Brazil, 203) National
1080 Wildlife Research Centre, Environment and Climate Change Canada, Carleton University, 1125 Colonel by Drive, Ottawa, ON K1A 0H3,
1081 Canada, 204) School of Life and Environmental Sciences, Deakin University, Burwood, Victoria, Australia, 3125, 205) Institute for Alpine
1082 Environment, Eurac Research, Viale Druso 1, 39100 Bozen/Bolzano, Italy, 206) Institute of Biology, Dept. of Molecular Botany, University of
1083 Hohenheim, 70599 Stuttgart, Germany, 207) Instituto de Matemática Aplicada San Luis, IMASL, CONICET and Universidad Nacional de San
1084 Luis, Ejército de los Andes 950, D5700HHW San Luis, Argentina, 208) Cátedra de Climatología Agrícola (FCA-UNER), Ruta 11, km 10, Oro
1085 Verde, Entre Ríos, Argentina, 209) Grupo de Ecología de Invasiones, INIBIOMA, CONICET/ Universidad Nacional del Comahue, Av. de los
1086 Pioneros 2350, Bariloche 8400, Argentina, 210) CSIC, Global Ecology Unit CREA- CSIC-UAB, Bellaterra, 08193, Catalonia, Spain., 211)
1087 CREA, E08193, Cerdanya del Vallès, Catalonia, Spain, 212) Mountains of the Moon University, P.O Box 837, Fort Portal, Uganda, 213)
1088 National Agricultural Research Organisation, Mbarara Zonal Agricultural Research and Development Institute, P.O Box 389, Mbarara,
1089 Uganda, 214) Department of Agroecology, Aarhus University, Blichers Allé 20, 8830 Tjele, Denmark, 215) Department of Biology, Lund
1090 University, SE-223 62 Lund, Sweden, 216) Department of Earth and Environmental Sciences, University of Pavia, Via S. Epifanio 14, 27100
1091 Pavia, Italy, 217) Institute of Botany and Landscape Ecology, University Greifswald, D-17487 Greifswald, Germany, 218) V.N. Sukachev
1092 Institute of Forest SB RAS, Krasnoyarsk, Russia, 219) Institute of Ecology and Earth Sciences, University of Tartu, Lai 40, Tartu 51005,
1093 Estonia, 220) Department of Biology , Aarhus University, Ole Worms Allé 1, 8000 Aarhus C, Denmark, 221) Department of Biology and
1094 Ecology Center, Utah State University, 5305 Old Main Hill, Logan, UT 84322, USA, 222) Department of Life Sciences, Imperial College,
1095 Silwood Park Campus, Ascot, Berkshire SL5 7PY, UK, 223) Landscape Ecology, Institute of Terrestrial Ecosystems, Department of
1096 Environmental Systems Science, ETH Zürich, 8092 Zürich, Switzerland, 224) Unit of Land Change Science, Swiss Federal Research Institute
1097 WSL, 8903 Birmensdorf, Switzerland, 225) Department of Biology, Washington University in St. Louis, Campus Box 1137, 1 Brookings Drive,
1098 St. Louis, MO 63130 USA, 226) School of Ecology and Environment Studies, Nalanda University, Rajgir, India, 227) Department of Animal
1099 and Plant Sciences, University of Sheffield, Western Bank, Sheffield, S10 2TN, U.K., 228) CESAM & Department of Environment, University
1100 of Aveiro, 3810-193 Aveiro, Portugal, 229) Department of Agronomy, Food, Natural resources, Animals and Environment - University of
1101 Padua, 35020 Legnaro, Italy, 230) Univ. Savoie Mont Blanc, CNRS, Univ. Grenoble Alpes, EDYTEM, F-73000 Chambéry, France, 231)
1102 Universitat Autònoma de Barcelona, E08193 Bellaterra (Cerdanya del Vallès), Catalonia, Spain, 232) Department of Ecology and
1103 Biogeography, Faculty of Biological and Veterinary Sciences, Nicolaus Copernicus University, Toruń, Poland, 233) Centre for Climate
1104 Change Research, Nicolaus Copernicus University, Toruń, Poland, 234) A. Borza Botanic Garden, Babeş-Bolyai University, Cluj-Napoca,
1105 Romania, 235) Faculty of Biology and Geology, Department of Taxonomy and Ecology, Babeş-Bolyai University, Cluj-Napoca, Romania, 236)
1106 E. G. Racoviță Institute, Babeş-Bolyai University, Cluj-Napoca, Romania, 237) Centre for Sustainable Ecosystem Solutions, School of Earth,
1107 Atmospheric and Life Sciences, University of Wollongong, Wollongong, New South Wales, 2522, Australia, 238) University of Applied
1108 Sciences Trier, Environmental Campus Birkenfeld, 55761 Birkenfeld, Germany, 239) Institut Universitaire de France, 1 Rue Descartes,
1109 75231 Paris cedex 05, France, 240) Swiss Federal Institute for Forest, Snow and Landscape Research WSL, Zuercherstrasse 111, 8903
1110 Birmensdorf, Switzerland, 242) Aquatic Ecology & Environmental Biology, Institute for Water and Wetland Research, Faculty of Science,
1111 Radboud University Nijmegen, AJ 6525 Nijmegen, The Netherlands., 243) University of Notre Dame, Department of Biological Sciences and
1112 the Environmental Change Initiative, 244) Swiss National Park, Chastè Planta-Wildenberg, 7530 Zernez, Switzerland, 245) Remote Sensing
1113 Laboratories, Dept. of Geography, University of Zurich, Winterthurerstrasse 190, 8057 Zurich, Switzerland, 246) CIRAD, UMR Eco&Sols,
1114 BP1386, CP18524, Dakar, Senegal, 247) Eco&Sols, Univ Montpellier, CIRAD, INRAE, IRD, Institut Agro, Montpellier, France, 248) LMI IESOL,
1115 Centre IRD-ISRA de Bel Air, BP1386, CP18524, Dakar, Senegal, 249) Parc national des Ecrins - Domaine de Charance - 05000 GAP - France,
1116 250) Universidad Nacional de San Antonio Abad del Cusco, Cusco, Perú, 251) Centro de Investigación de la Biodiversidad Wilhelm L.
1117 Johannsen, Cusco, Perú, 252) Biological Dynamics of Forest Fragments Project, PDBFF, Instituto Nacional de Pesquisas da Amazônia, Av.
1118 André Araujo, 2936 - Petrópolis, Manaus, Amazonas, 69067-375, Brazil, 253) Department of Ecology and Environmental Science, Umeå
1119 University, 901 87 Umeå, Sweden, 254) Institute of Bio- and Geosciences (IBG-3): Agrosphere, Forschungszentrum Jülich GmbH, Jülich,
1120 Germany, 255) Chair of Soil Science and Geomorphology, Department of Geosciences, University of Tuebingen, 72070 Tuebingen,
1121 Germany, 256) Department of Geography, The University of British Columbia, Vancouver, BC V6T 1Z2, 257) Department of Ecology,
1122 University of Innsbruck, Technikerstrasse 25, 6020 Innsbruck, Austria, 258) Department of Botany and Biodiversity Research, Rennweg 14,
1123 1030 Vienna, 259) Princeton School of Public and International Affairs, Princeton University, Princeton, NJ 08540, USA, 260) Université de
1124 Lorraine, AgroParisTech, INRAE, Silva, 54000 Nancy, France., 261) Department of Soil Science and Landscape Management, Faculty of
1125 Earth Sciences and Spatial Management, Nicolaus Copernicus University, Toruń, Poland, 262) Terra Nova National Park, Parks Canada
1126 Agency, Glovertown NL, A0G3Y0, 263) Universidade Estadual do Norte Fluminense Darcy Ribeiro, Campos dos Goytacazes, Rio de Janeiro,
1127 Brazil, 264) National Forest Centre, Forest Research Institute Zvolen, T. G. Masaryka 22, 96001 Zvolen, Slovakia, 265) Asian School of
1128 Environment, Nanyang Technological University, 42 Nanyang Ave, Singapore 639815, Singapore, 266) Department of Geography,
1129 University of British Columbia, 1984 West Mall, Vancouver, BC V6T 1Z2, 267) Department of Earth and Environmental Sciences,
1130 Celestijnenlaan 200E, 3001 Leuven, Belgium, 268) Universidade Federal da Paraíba, Departamento de Geociências. Cidade Universitária,
1131 João Pessoa - PB, CEP 58051-900, Brasil, 269) Goethe-Universität Frankfurt, Department of Physical Geography, Altenhöferallee 1, 60438

1132 Frankfurt am Main, Germany, 270) Department of Evolution, Ecology, and Organismal Biology, University of California Riverside, Riverside,
1133 CA, 92521, USA, 271) Department of Natural History, NTNU University Museum, Norwegian University of Science and Technology, NO-
1134 7491 Trondheim Norway, 272) UR 'Ecologie et Dynamique des Systèmes Anthropisées' (EDYSAN, UMR 7058 CNRS-UPJV), Univ. de Picardie
1135 Jules Verne, Amiens, France, 273) EnvixLab, Dipartimento di Bioscienze e Territorio, Università degli Studi del Molise, Via Duca degli
1136 Abruzzi s.n.c., 86039 Termoli, Italy, 274) Institute of Meteorology and Climate Research (IMK), Department of Atmospheric Environmental
1137 Reserach (IFU), Karlsruhe Institute of Technology (KIT), Kreuzeckbahn Straße 19, 82467 Garmisch-Partenkirchen, Germany, 275) Swedish
1138 University of Agricultural Sciences, SLU Swedish Species Information Centre, Almas allé 8 E, 75651 Uppsala, Sweden, 276) University
1139 Duisburg-Essen, Faculty for Biology, Universitätsstr. 5, 45141 Essen, Germany, 277) Department of Geosciences and Natural Resource
1140 Management, University of Copenhagen, Øster Voldgade 10, DK-1350 Copenhagen, Denmark, 278) Experimental Plant Ecology, Institute
1141 of Botany and Landscape Ecology, University of Greifswald, partner in the Greifswald Mire Centre, D-17487 Greifswald, Germany, 279)
1142 Fondation J.-M. Aubert, 1938 Champex-Lac, Switzerland, 280) Département de Botanique et Biologie végétale, Université de Genève, Case
1143 postale 71, CH-1292 Chambésy, Switzerland, 281) Department of Geography and Earth Sciences, Aberystwyth University, Wales, UK, 282)
1144 Center for Systematic Biology, Biodiversity and Bioresources - 3B, Babeş-Bolyai University, Cluj-Napoca, Romania, 283) Northern
1145 Environmental Geoscience Laboratory, Department of Geography and Planning, Queen's University, 284) Graduate School of Life and
1146 Environmental Sciences, Osaka Prefecture University, 599-8531, Japan, 285) Nature Research Centre, Akademijos 2, 08412 Vilnius,
1147 Lithuania, 286) Institute of Biological Research Cluj-Napoca, National Institute of Research and Development for Biological Sciences,
1148 Bucharest, Romania, 287) CNR Institute for BioEconomy, Via Giovanni Caproni, 50144 Firenze, Italy, 288) The Ecosystem Management
1149 Research Group (ECOBE), University of Antwerp, 2610 Wilrijk (Antwerpen), Belgium, 289) Plant Conservation and Population Biology,
1150 Department of Biology, KU Leuven, Kasteelpark Arenberg 31, 3001 Heverlee, Belgium, 290) A.N. Severtsov Institute of Ecology and
1151 Evolution, Russian Academy of Sciences, 119071, Leninsky pr.33, Moscow, Russia, 291) Netherlands Institute of Ecology,
1152 Droevedaalsesteeg 10, 6708 PB, Wageningen, 292) Plant Ecology & Nature Conservation Group Wageningen University , Droevedaalse
1153 Steeg 3a 6708 PB Wageningen, 293) Centre for Integrative Ecology, School of Life and Environmental Sciences, Deakin University,
1154 Burwood, Victoria, Australia, 3125, 294) CAVElab - Computational and Applied Vegetation Ecology, Department of Environment, Ghent
1155 University, Coupure Links 653, 9000 Gent, Belgium, 295) Earth Surface Processes Team, Centre for Environmental and Marine Studies
1156 (CESAM), Dept. Environment and Planning, University of Aveiro, 3810-193, Aveiro, Portugal, 296) Instituto Pirenaico de Ecología, IPE-CSIC.
1157 Av. Llano de la Victoria, 16. 22700 Jaca (Huesca) Spain, 297) CNR - Institute for Agricultural and Forestry Systems in the Mediterranean,
1158 P.le Enrico Fermi 1- Loc. del Granatello, 80055, Portici, (Napoli), Italy, 298) Institute of Earth Surface Dynamics, Faculty of Geosciences and
1159 Environment, University of Lausanne, Géopolis, 1015 Lausanne, Switzerland, 299) Forest Research, Northern Research Station, Roslin,
1160 EH25 9SY, UK, 300) Institute of Mountain Hazards and Environment, Chinese Academy of Sciences, Chengdu, P.R. China, 301) Department
1161 of Earth and Environmental Sciences, Lehigh University, Bethlehem, PA 18015, United States, 302) Institute for Peat and Mire Research,
1162 School of Geographical Sciences, Northeast Normal University, Changchun, Jilin 130024, China, 303) High Meadows Environmental
1163 Institute, Princeton University, NJ 08544, USA, 304) Zhejiang Tiantong Forest Ecosystem National Observation and Research Station,
1164 School of Ecological and Environmental Sciences, East China Normal University, Shanghai 200241, China, 305) JJL received funding from
1165 the National Natural Science Foundation of China (grant nr. 32071538), 306) University of Bayreuth, Ecological-Botanical Gardens,
1166 Universitätsstr. 30, Bayreuth, Germany, 307) Key Laboratory of Geographical Processes and Ecological Security in Changbai Mountains,
1167 Ministry of Education, School of Geographical Sciences, Northeast Normal University, Changchun 130024, China

1168

1169 References

1170 Abatzoglou JT, Dobrowski SZ, Parks SA, Hegewisch KC (2018) TerraClimate, a high-resolution global
1171 dataset of monthly climate and climatic water balance from 1958–2015. *Scientific data*, **5**,
1172 170191.

1173 Amatulli G, Domisch S, Tuanmu M-N, Parmentier B, Ranipeta A, Malczyk J, Jetz W (2018) A suite of
1174 global, cross-scale topographic variables for environmental and biodiversity modeling.
1175 *Scientific data*, **5**, 180040.

1176 Antão LH, Bates AE, Blowes SA, Waldock C, Supp SR, Magurran AE, Dornelas M, Schipper AM (2020)
1177 Temperature-related biodiversity change across temperate marine and terrestrial systems.
1178 *Nature ecology & evolution*, **4**, 927-933.

1179 Ashcroft MB, Cavanagh M, Eldridge MDB, Gollan JR (2014) Testing the ability of topoclimatic grids of
1180 extreme temperatures to explain the distribution of the endangered brush-tailed rock-
1181 wallaby (*Petrogale penicillata*). *Journal of biogeography*, **41**, 1402-1413.

1182 Ashcroft MB, Chisholm LA, French KO (2008) The effect of exposure on landscape scale soil surface
1183 temperatures and species distribution models. *Landscape Ecology*, **23**, 211-225.

1184 Ashcroft MB, Gollan JR (2012) Fine-resolution (25 m) topoclimatic grids of near-surface (5 cm)
1185 extreme temperatures and humidities across various habitats in a large (200 x 300 km) and
1186 diverse region. *International Journal of Climatology*, **32**, 2134-2148.

1187 Barnes R, Sahr K, Evenden G, Johnson A, Warmerdam F (2017) dggridR: discrete global grids for R. R
1188 package version 0.1.12.

1189 Bergstrom DM, Wienecke BC, Van Den Hoff J, Hughes L, Lindenmayer DB, Ainsworth TD, Baker CM,
1190 Bland L, Bowman DM, Brooks ST (2021) Combating ecosystem collapse from the tropics to
1191 the Antarctic. *Global change biology*, **27**, 1692-1703.

1192 Berner LT, Massey R, Jantz P, Forbes BC, Macias-Fauria M, Myers-Smith I, Kumpula T, Gauthier G,
1193 Andreu-Hayles L, Gaglioti BV (2020) Summer warming explains widespread but not uniform
1194 greening in the Arctic tundra biome. *Nature Communications*, **11**, 1-12.

1195 Bond-Lamberty B, Thomson A (2018) A Global Database of Soil Respiration Data, Version 4.0. ORNL
1196 DAAC.

1197 Booth TH, Nix HA, Busby JR, Hutchinson MF (2014) BIOCLIM: the first species distribution modelling
1198 package, its early applications and relevance to most current MAXENT studies. *Diversity and
1199 Distributions*, **20**, 1-9.

1200 Bramer I, Anderson B, Bennie J, Bladon A, De Frenne P, Hemming D, Hill RA, Kearney MR, Körner C,
1201 Korstjens AH, Lenoir J, Maclean IMD, Marsh CD, Morecroft MD, Ohlemüller R, Slater HD,
1202 Suggitt AJ, Zellweger F, Gillingham PK (2018) Advances in monitoring and modelling climate
1203 at ecologically relevant scales. *Advances in Ecological Research*, **58**, 101-161.

1204 Bruelheide H, Dengler J, Purschke O, Lenoir J, Jiménez-Alfaro B, Hennekens SM, Botta-Dukát Z,
1205 Chytrý M, Field R, Jansen F (2018) Global trait–environment relationships of plant
1206 communities. *Nature ecology & evolution*, **2**, 1906.

1207 Bütkofer L, Anderson K, Bebber DP, Bennie JJ, Early RI, Maclean IM (2020) The problem of scale in
1208 predicting biological responses to climate. *Global change biology*, **26**, 6657-6666.

1209 Chen L, Aalto J, Luoto M (2021) Significant shallow–depth soil warming over Russia during the past
1210 40 years. *Global and Planetary Change*, **197**, 103394.

1211 Cooper EJ (2014) Warmer shorter winters disrupt Arctic terrestrial ecosystems. *Annual Review of
1212 Ecology, Evolution, and Systematics*, **45**, 271-295.

1213 Copernicus Climate Change Service (C3s) (2019) C3S ERA5-Land reanalysis. (ed Copernicus Climate
1214 Change Service).

1215 Coûteaux M-M, Bottner P, Berg B (1995) Litter decomposition, climate and litter quality. *Trends in
1216 ecology & evolution*, **10**, 63-66.

1217 Crowther TW, Todd-Brown KE, Rowe CW, Wieder WR, Carey JC, Machmuller MB, Snoek B, Fang S,
1218 Zhou G, Allison SD (2016) Quantifying global soil carbon losses in response to warming.
1219 *Nature*, **540**, 104-108.

1220 Daly C (2006) Guidelines for assessing the suitability of spatial climate data sets. International
1221 Journal of Climatology, **26**, 707-721.

1222 Davis E, Trant A, Hermanutz L, Way RG, Lewkowicz AG, Collier LS, Cuerrier A, Whitaker D (2020)
1223 Plant–Environment Interactions in the Low Arctic Torngat Mountains of Labrador.
1224 Ecosystems, 1-21.

1225 De Frenne P, Lenoir J, Luoto M, Scheffers BR, Zellweger F, Aalto J, Ashcroft M, Christiansen D,
1226 Decocq G, De Pauw K, Govaert S, Greiser C, Gril E, Hampe A, Jucker T, Klinge D, Koelemeijer
1227 I, Lembrechts J, Marrec R, Meeussen C, Ogee J, Tyystjarvi V, Vangansbeke P, Hylander K
1228 (2021) Forest microclimates and climate change: importance, drivers and future research
1229 agenda. Global change biology, **In press**.

1230 De Frenne P, Rodríguez-Sánchez F, Coomes DA, Baeten L, Verstraeten G, Vellend M, Bernhardt-
1231 Römermann M, Brown CD, Brunet J, Cornelis J (2013) Microclimate moderates plant
1232 responses to macroclimate warming. Proceedings of the National Academy of Sciences, **110**,
1233 18561-18565.

1234 De Frenne P, Zellweger F, Rodríguez-Sánchez F, Scheffers BR, Hylander K, Luoto M, Vellend M,
1235 Verheyen K, Lenoir J (2019) Global buffering of temperatures under forest canopies. Nature
1236 ecology & evolution, **3**, 744-749.

1237 Dinerstein E, Olson D, Joshi A, Vynne C, Burgess ND, Wikramanayake E, Hahn N, Palminteri S, Hedao
1238 P, Noss R (2017) An ecoregion-based approach to protecting half the terrestrial realm.
1239 BioScience, **67**, 534-545.

1240 Du E, Terrer C, Pellegrini AF, Ahlström A, Van Lissa CJ, Zhao X, Xia N, Wu X, Jackson RB (2020) Global
1241 patterns of terrestrial nitrogen and phosphorus limitation. Nature Geoscience, **13**, 221-226.

1242 Fick SE, Hijmans RJ (2017) WorldClim 2: new 1-km spatial resolution climate surfaces for global land
1243 areas. International Journal of Climatology, **37**, 4302-4315.

1244 Geiger R (1950) *The climate near the ground*, Cambridge, Massachusetts, USA, Harvard University
1245 Press.

1246 Gistemp Team (2021) GISS Surface Temperature Analysis (GISTEMP), version 4. NASA Goddard
1247 Institute for Space Studies.

1248 Gorelick N, Hancher M, Dixon M, Ilyushchenko S, Thau D, Moore R (2017) Google Earth Engine:
1249 Planetary-scale geospatial analysis for everyone. Remote Sensing of Environment, **202**, 18-
1250 27.

1251 Gottschall F, Davids S, Newiger-Dous TE, Auge H, Cesatz S, Eisenhauer N (2019) Tree species identity
1252 determines wood decomposition via microclimatic effects. Ecology and evolution, **9**, 12113-
1253 12127.

1254 Graae BJ, Vandvik V, Armbruster WS, Eiserhardt WL, Svenning J-C, Hylander K, Ehrlén J, Speed JD,
1255 Klanderud K, Bråthen KA, Milbau A, Opedal OH, Alsoe IG, Ejrnaes R, Bruun HH, Birks HJB,
1256 Westergaard KB, Birks HH, Lenoir J (2018) Stay or go—how topographic complexity influences
1257 alpine plant population and community responses to climate change. Perspectives in plant
1258 ecology, evolution and systematics, **30**, 41-50.

1259 Greiser C, Meineri E, Luoto M, Ehrlén J, Hylander K (2018) Monthly microclimate models in a
1260 managed boreal forest landscape. Agricultural and Forest Meteorology, **250**, 147-158.

1261 Grünberg I, Wilcox EJ, Zwieback S, Marsh P, Boike J (2020) Linking tundra vegetation, snow, soil
1262 temperature, and permafrost. Biogeosciences, **17**, 4261-4279.

1263 Grundstein A, Todhunter P, Mote T (2005) Snowpack control over the thermal offset of air and soil
1264 temperatures in eastern North Dakota. Geophysical Research Letters, **32**.

1265 Hall DK, Riggs GA, Salomonson VV, Digirolamo NE, Bayr KJ (2002) MODIS snow-cover products.
1266 Remote Sensing of Environment, **83**, 181-194.

1267 Hengl T, De Jesus JM, Heuvelink GB, Gonzalez MR, Kilibarda M, Blagotić A, Shangguan W, Wright
1268 MN, Geng X, Bauer-Marschallinger B (2017) SoilGrids250m: Global gridded soil information
1269 based on machine learning. Plos One, **12**, e0169748.

1270 Hengl T, Nussbaum M, Wright MN, Heuvelink GB, Gräler B (2018) Random forest as a generic
1271 framework for predictive modeling of spatial and spatio-temporal variables. *PeerJ*, **6**, e5518.

1272 Hennon PE, D'amore DV, Witter DT, Lamb MB (2010) Influence of forest canopy and snow on
1273 microclimate in a declining yellow-cedar forest of Southeast Alaska. *Northwest Science*, **84**,
1274 73-87.

1275 Holden ZA, Klene AE, Keefe RF, Moisen GG (2013) Design and evaluation of an inexpensive radiation
1276 shield for monitoring surface air temperatures. *Agricultural and Forest Meteorology*, **180**,
1277 281-286.

1278 Hursh A, Ballantyne A, Cooper L, Maneta M, Kimball J, Watts J (2017) The sensitivity of soil
1279 respiration to soil temperature, moisture, and carbon supply at the global scale. *Global
1280 change biology*, **23**, 2090-2103.

1281 Jian J, Steele MK, Zhang L, Bailey VL, Zheng J, Patel KF, Bond-Lamberty BP (2021) On the use of air
1282 temperature and precipitation as surrogate predictors in soil respiration modelling.
1283 *European Journal of Soil Science*.

1284 Johnston AS, Meade A, Ardö J, Arriga N, Black A, Blanken PD, Bonal D, Brümmer C, Cescatti A, Dušek
1285 J (2021) Temperature thresholds of ecosystem respiration at a global scale. *Nature ecology
1286 & evolution*, **5**, 487-494.

1287 Karger DN, Conrad O, Böhner J, Kawohl T, Kreft H, Soria-Auza RW, Zimmermann NE, Linder HP,
1288 Kessler M (2017a) Climatologies at high resolution for the earth's land surface areas.
1289 *Scientific data*, **4**, 170122.

1290 Karger DN, Conrad O, Böhner J, Kawohl T, Kreft H, Soria-Auza RW, Zimmermann NE, Linder HP,
1291 Kessler M (2017b) Data from: Climatologies at high resolution for the earth's land surface
1292 areas. In: *Dryad Digital Repository*.

1293 Kattge J, Bönisch G, Diaz S, Lavorel S, Prentice IC, Leadley P, Tautenhahn S, Werner G, Günther A
1294 (2019) TRY plant trait database-enhanced coverage and open access. *Global change biology*,
1295 **26**, 119-188.

1296 Kearney M, Porter W (2009) Mechanistic niche modelling: combining physiological and spatial data
1297 to predict species' ranges. *Ecology letters*, **12**, 334-350.

1298 Kearney M, Shine R, Porter WP (2009) The potential for behavioral thermoregulation to buffer "cold-
1299 blooded" animals against climate warming. *Proceedings of the National Academy of
1300 Sciences*, **106**, 3835-3840.

1301 Kearney MR, Gillingham PK, Bramer I, Duffy JP, Maclean IM (2019) A method for computing hourly,
1302 historical, terrain-corrected microclimate anywhere on Earth. *Methods in Ecology and
1303 Evolution*, **11**, 38-43.

1304 Kissling WD, Walls R, Bowser A, Jones MO, Kattge J, Agosti D, Amengual J, Basset A, Van Bodegom
1305 PM, Cornelissen JH (2018) Towards global data products of Essential Biodiversity Variables
1306 on species traits. *Nature ecology & evolution*, **2**, 1531-1540.

1307 Körner C, Hiltbrunner E (2018) The 90 ways to describe plant temperature. *Perspectives in plant
1308 ecology, evolution and systematics*, **30**, 16-21.

1309 Körner C, Paulsen J (2004) A world-wide study of high altitude treeline temperatures. *Journal of
1310 biogeography*, **31**, 713-732.

1311 Lembrechts J, Aalto J, Ashcroft M, De Frenne P, Kopecký M, Lenoir J, Luoto M, Maclean IM,
1312 Consortium S, Nijs I (2020) SoilTemp: call for data for a global database of near-surface
1313 temperature. *Global change biology*, **26**, 6616-6629.

1314 Lembrechts J, Lenoir J, Scheffers BR, De Frenne P (2021) Time for countrywide microclimate
1315 networks. *Global Ecology and Biogeography*.

1316 Lembrechts JJ, Lenoir J (2019) Microclimatic conditions anywhere at any time! *Global change
1317 biology*.

1318 Lembrechts JJ, Lenoir J, Roth N, Hattab T, Milbau A, Haider S, Pellissier L, Pauchard A, Ratier Backes
1319 A, Dimarco RD (2019) Comparing temperature data sources for use in species distribution

1320 models: From in-situ logging to remote sensing. *Global Ecology and Biogeography*, **28**, 1578-
1321 1596.

1322 Lembrechts JJ, Nijs I (2020) Microclimate shifts in a dynamic world. *Science*, **368**, 711-712.

1323 Lenoir J, Bertrand R, Comte L, Bourgeaud L, Hattab T, Murienne J, Grenouillet G (2020) Species
1324 better track climate warming in the oceans than on land. *Nature ecology & evolution*, **4**,
1325 1044-1059.

1326 Luoju K, Pulliainen J, Takala M, Derksen C, Rott H, Nagler T, Solberg R, Wiesmann A, Metsamaki S,
1327 Malnes E (2010) Investigating the feasibility of the GlobSnow snow water equivalent data for
1328 climate research purposes. In: *2010 IEEE International Geoscience and Remote Sensing
1329 Symposium*. IEEE.

1330 Maclean IM, Duffy JP, Haesen S, Govaert S, De Frenne P, Vanneste T, Lenoir J, Lembrechts JJ, Rhodes
1331 MW, Van Meerbeek K (2021) On the measurement of microclimate. *Methods in Ecology and
1332 Evolution*.

1333 Maclean IM, Klings DH (2021) Microclimc: A mechanistic model of above, below and within-canopy
1334 microclimate. *Ecological Modelling*, **451**, 109567.

1335 Maclean IM, Mosedale JR, Bennie JJ (2019) Microclima: An r package for modelling meso-and
1336 microclimate. *Methods in Ecology and Evolution*, **10**, 280-290.

1337 Myers-Smith IH, Kerby JT, Phoenix GK, Bjerke JW, Epstein HE, Assmann JJ, John C, Andreu-Hayles L,
1338 Angers-Blondin S, Beck PS (2020) Complexity revealed in the greening of the Arctic. *Nature
1339 Climate Change*, **10**, 106-117.

1340 Niittynen P, Heikkinen RK, Aalto J, Guisan A, Kemppinen J, Luoto M (2020) Fine-scale tundra
1341 vegetation patterns are strongly related to winter thermal conditions. *Nature Climate
1342 Change*, **10**, 1143-1148.

1343 Niittynen P, Luoto M (2018) The importance of snow in species distribution models of arctic
1344 vegetation. *Ecography*, **41**, 1024-1037.

1345 O'donnell MS, Ignizio DA (2012) Bioclimatic predictors for supporting ecological applications in the
1346 conterminous United States. *US Geological Survey Data Series*, **691**, 4-9.

1347 Obu J, Westermann S, Bartsch A, Berdnikov N, Christiansen HH, Dashtseren A, Delaloye R, Elberling
1348 B, Etzelmüller B, Kholodov A (2019) Northern Hemisphere permafrost map based on TTOP
1349 modelling for 2000–2016 at 1 km² scale. *Earth-Science Reviews*, **193**, 299-316.

1350 Olden JD, Lawler JJ, Poff NL (2008) Machine learning methods without tears: a primer for ecologists.
1351 *The Quarterly review of biology*, **83**, 171-193.

1352 Opdal OH, Armbruster WS, Graae BJ (2015) Linking small-scale topography with microclimate, plant
1353 species diversity and intra-specific trait variation in an alpine landscape. *Plant Ecology &
1354 Diversity*, **8**, 305-315.

1355 Overland JE, Wang M, Walsh JE, Stroeve JC (2014) Future Arctic climate changes: Adaptation and
1356 mitigation time scales. *Earth's Future*, **2**, 68-74.

1357 Pastorello G, Papale D, Chu H, Trotta C, Agarwal D, Canfora E, Baldocchi D, Torn M (2017) A new data
1358 set to keep a sharper eye on land-air exchanges. *Eos, Transactions American Geophysical
1359 Union (Online)*, **98**.

1360 Perera-Castro AV, Waterman MJ, Turnbull JD, Ashcroft MB, Mckinley E, Watling JR, Bramley-Alves J,
1361 Casanova-Katny A, Zuniga G, Flexas J (2020) It is hot in the sun: Antarctic mosses have high
1362 temperature optima for photosynthesis despite cold climate. *Frontiers in Plant Science*, **11**,
1363 1178.

1364 Pincebourde S, Murdock CC, Vickers M, Sears MW (2016) Fine-scale microclimatic variation can
1365 shape the responses of organisms to global change in both natural and urban environments.
1366 *Integrative and Comparative Biology*, **56**, 45-61.

1367 Pleim JE, Gilliam R (2009) An indirect data assimilation scheme for deep soil temperature in the
1368 Pleim–Xiu land surface model. *Journal of Applied Meteorology and Climatology*, **48**, 1362-
1369 1376.

1370 Portillo-Estrada M, Pihlatie M, Korhonen JFJ, Levula J, Frumau AKF, Ibrom A, Lembrechts JJ, Morillas
1371 L, Horvath L, Jones SK, Niinemets U (2016) Climatic controls on leaf litter decomposition
1372 across European forests and grasslands revealed by reciprocal litter transplantation
1373 experiments. *Biogeosciences*, **13**, 1621-1633.

1374 Potter KA, Woods HA, Pincebourde S (2013) Microclimatic challenges in global change biology.
1375 *Global change biology*, **19**, 2932-2939.

1376 R Core Team (2020) R: a language and environment for statistical computing, R Foundation for
1377 Statistical Computing.

1378 Richardson LF (1922) *Weather prediction by numerical process*, Cambridge university press.

1379 Rosenberg NJ, Kimball B, Martin P, Cooper C (1990) From climate and CO₂ enrichment to
1380 evapotranspiration. *Climate change and US water resources.*, 151-175.

1381 Santoro M (2018) GlobBiomass—Global datasets of forest biomass. PANGAEA10, **1594**.

1382 Scherrer D, Schmid S, Körner C (2011) Elevational species shifts in a warmer climate are
1383 overestimated when based on weather station data. *International journal of*
1384 *Biometeorology*, **55**, 645-654.

1385 Schimel DS, Braswell B, McKeown R, Ojima DS, Parton W, Pulliam W (1996) Climate and nitrogen
1386 controls on the geography and timescales of terrestrial biogeochemical cycling. *Global*
1387 *Biogeochemical Cycles*, **10**, 677-692.

1388 Schimel JP, Bilbrough C, Welker JM (2004) Increased snow depth affects microbial activity and
1389 nitrogen mineralization in two Arctic tundra communities. *Soil Biology and Biochemistry*, **36**,
1390 217-227.

1391 Senior RA, Hill JK, Edwards DP (2019) Global loss of climate connectivity in tropical forests. *Nature*
1392 *Climate Change*, **9**, 623-626.

1393 Smith M, Riseborough D (1996) Permafrost monitoring and detection of climate change. *Permafrost*
1394 and Periglacial Processes, **7**, 301-309.

1395 Smith M, Riseborough D (2002) Climate and the limits of permafrost: a zonal analysis. *Permafrost*
1396 and Periglacial Processes, **13**, 1-15.

1397 Soudzilovskaia NA, Douma JC, Akhmetzhanova AA, Van Bodegom PM, Cornwell WK, Moens EJ,
1398 Treseder KK, Tibbitt M, Wang YP, Cornelissen JH (2015) Global patterns of plant root
1399 colonization intensity by mycorrhizal fungi explained by climate and soil chemistry. *Global*
1400 *Ecology and Biogeography*, **24**, 371-382.

1401 Stefan V, Levin S (2018) Plotbiomes: Plot Whittaker biomes with ggplot2. R package version 0.0.
1402 0.9001.

1403 Steidinger BS, Crowther TW, Liang J, Van Nuland ME, Werner GD, Reich PB, Nabuurs G-J, De-Miguel
1404 S, Zhou M, Picard N (2019) Climatic controls of decomposition drive the global biogeography
1405 of forest-tree symbioses. *Nature*, **569**, 404-408.

1406 Terando AJ, Youngsteadt E, Meineke EK, Prado SG (2017) Ad hoc instrumentation methods in
1407 ecological studies produce highly biased temperature measurements. *Ecology and evolution*,
1408 **7**, 9890-9904.

1409 Van Den Hoogen J, Geisen S, Routh D, Ferris H, Traunspurger W, Wardle DA, De Goede RG, Adams
1410 BJ, Ahmad W, Andriuzzi WS (2019) Soil nematode abundance and functional group
1411 composition at a global scale. *Nature*, **572**, 194-198.

1412 Van Den Hoogen J, Robmann N, Routh D, Lauber T, Van Tiel N, Danylo O, Crowther TW (2021) A
1413 geospatial mapping pipeline for ecologists. *bioRxiv*,
1414 <https://doi.org/10.1101/2021.07.07.451145>.

1415 Wang K, Dickinson RE (2012) A review of global terrestrial evapotranspiration: Observation,
1416 modeling, climatology, and climatic variability. *Reviews of Geophysics*, **50**.

1417 Way RG, Lewkowicz AG (2018) Environmental controls on ground temperature and permafrost in
1418 Labrador, northeast Canada. *Permafrost and Periglacial Processes*, **29**, 73-85.

1419 White HJ, León-Sánchez L, Burton VJ, Cameron EK, Caruso T, Cunha L, Dirilgen T, Jurburg SD, Kelly R,
1420 Kumaresan D (2020) Methods and approaches to advance soil macroecology. *Global Ecology*
1421 and *Biogeography*, **29**, 1674-1690.

1422 Whiteman CD (1982) Breakup of temperature inversions in deep mountain valleys: Part I.
1423 Observations. *Journal of Applied Meteorology*, **21**, 270-289.

1424 Wild J, Kopecký M, Macek M, Šanda M, Jankovec J, Haase T (2019) Climate at ecologically relevant
1425 scales: A new temperature and soil moisture logger for long-term microclimate
1426 measurement. *Agricultural and Forest Meteorology*, **268**, 40-47.

1427 Wood S (2012) mgcv: Mixed GAM Computation Vehicle with GCV/AIC/REML smoothness estimation.

1428 World Meteorological Organization (2008) *Guide to Meteorological Instruments and Methods of*
1429 *Observation*, Geneva, WMO-No. 8.

1430 Xu T, Hutchinson M (2011) ANUCLIM version 6.1 user guide. The Australian National University,
1431 Fenner School of Environment and Society, Canberra.

1432 Xu Y, Ramanathan V, Victor DG (2018) Global warming will happen faster than we think. *Nature*.

1433 Zellweger F, De Frenne P, Lenoir J, Vangansbeke P, Verheyen K, Bernhardt-Römermann M, Baeten L,
1434 Hédl R, Berki I, Brunet J, Van Calster H, Chudomelová M, Decocq G, Dirnböck T, Durak T,
1435 Heiniken T, Jaroszewicz B, Kopecký M, Malis F, Macek M, Marek M, Naaf T, Nagel TA,
1436 Ortmann-Ajkai A, Petrik P, Pielech R, Reczynska K, Schmidt W, Standová T, Swierkosz K,
1437 Teleki B, Vild O, Wulf M, Coomes D (2020) Forest microclimate dynamics drive plant
1438 responses to warming. *Science*, **368**, 772-775.

1439 Zhang Y, Sherstiukov AB, Qian B, Kokelj SV, Lantz TC (2018) Impacts of snow on soil temperature
1440 observed across the circumpolar north. *Environmental Research Letters*, **13**, 044012.

1441 Zhang Y, Wang S, Barr AG, Black T (2008) Impact of snow cover on soil temperature and its
1442 simulation in a boreal aspen forest. *Cold Regions Science and Technology*, **52**, 355-370.

1443 Zhou S, Williams AP, Lintner BR, Berg AM, Zhang Y, Keenan TF, Cook BI, Hagemann S, Seneviratne SI,
1444 Gentile P (2021) Soil moisture–atmosphere feedbacks mitigate declining water availability
1445 in drylands. *Nature Climate Change*, 1-7.

1446 Zomer RJ, Trabucco A, Bossio DA, Verchot LV (2008) Climate change mitigation: A spatial analysis of
1447 global land suitability for clean development mechanism afforestation and reforestation.
1448 *Agriculture, ecosystems & environment*, **126**, 67-80.

1449
1450
1451
1452
1453
1454

1455 **Tables**

1456 **Table 1:** Overview of soil bioclimatic variables as calculated in this study.

Bioclimatic variable	Meaning
SBIO1	annual mean temperature
SBIO2	mean diurnal range (mean of monthly (max temp - min temp))
SBIO3	isothermality (SBIO2/SBIO7) ($\times 100$)
SBIO4	temperature seasonality (standard deviation $\times 100$)
SBIO5	max temperature of warmest month
SBIO6	min temperature of coldest month
SBIO7	temperature annual range (SBIO5-SBIO6)
SBIO8	mean temperature of wettest quarter
SBIO9	mean temperature of driest quarter
SBIO10	mean temperature of warmest quarter
SBIO11	mean temperature of coldest quarter

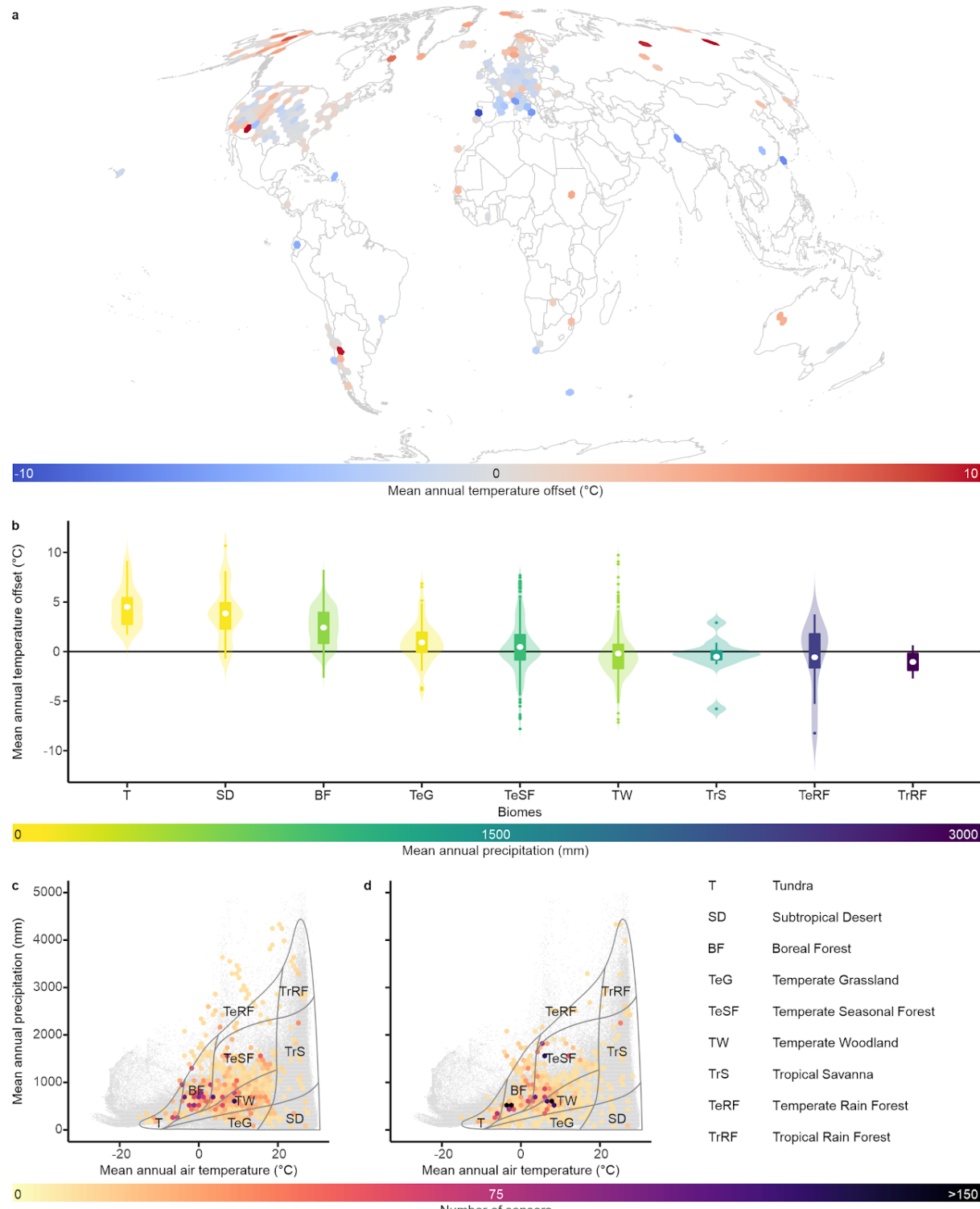
1457

1458

1459

1460 **Figure legends**

1461



1462

1463 **Figure 1: Temperature offsets between soil and air temperature differed significantly among**
1464 **biomes.** (a) Distribution of in-situ measurement locations across the globe, coloured by the mean

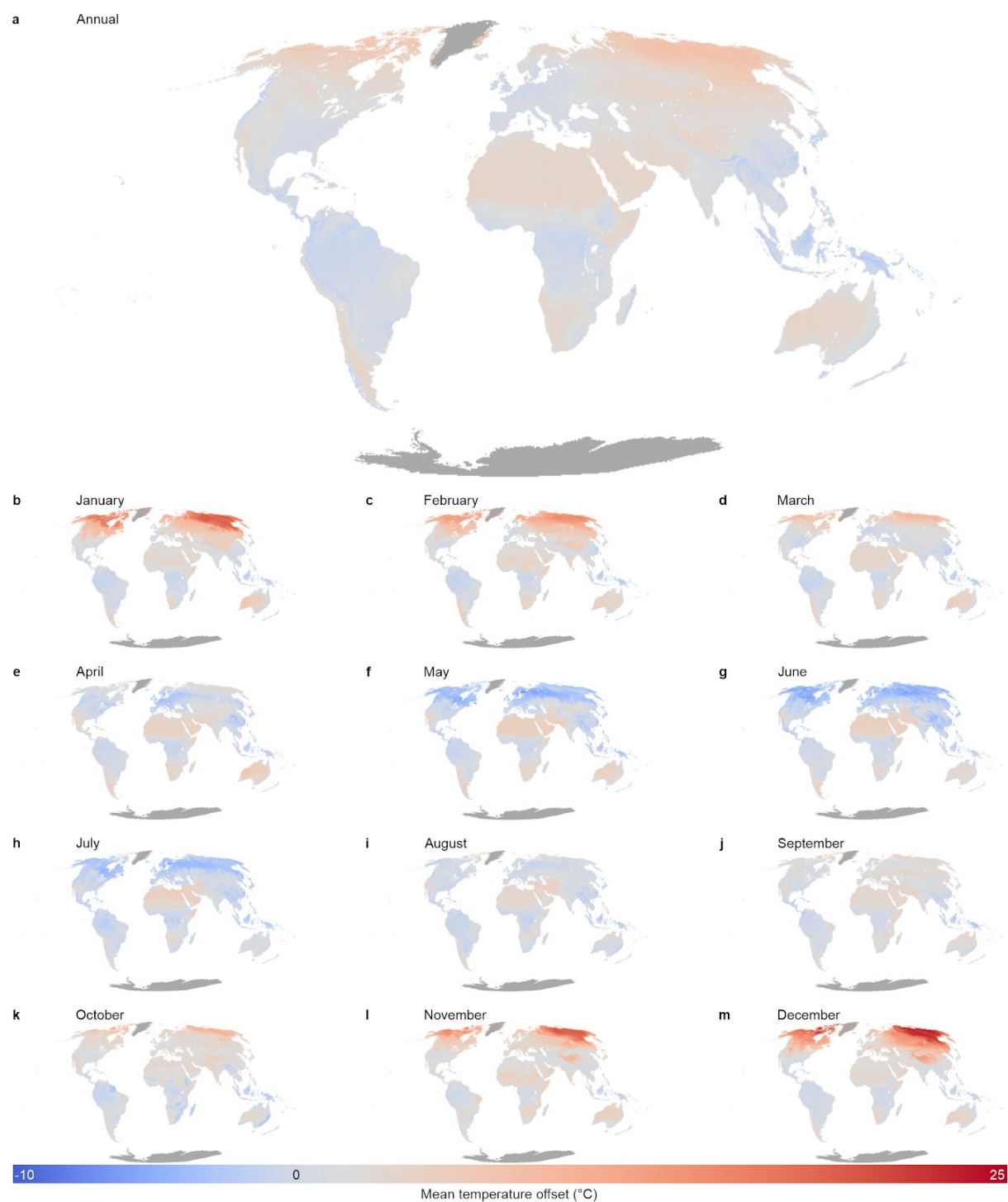
1465 annual temperature offset (in °C) between in situ measured soil temperature (topsoil, 0–5 cm depth)

1466 and gridded air temperature (ERA5L). Offsets were averaged per hexagon, each with a size of

1467 approximately 70,000 km². Mollweide projection. (b) Mean annual temperature offsets per Whittaker

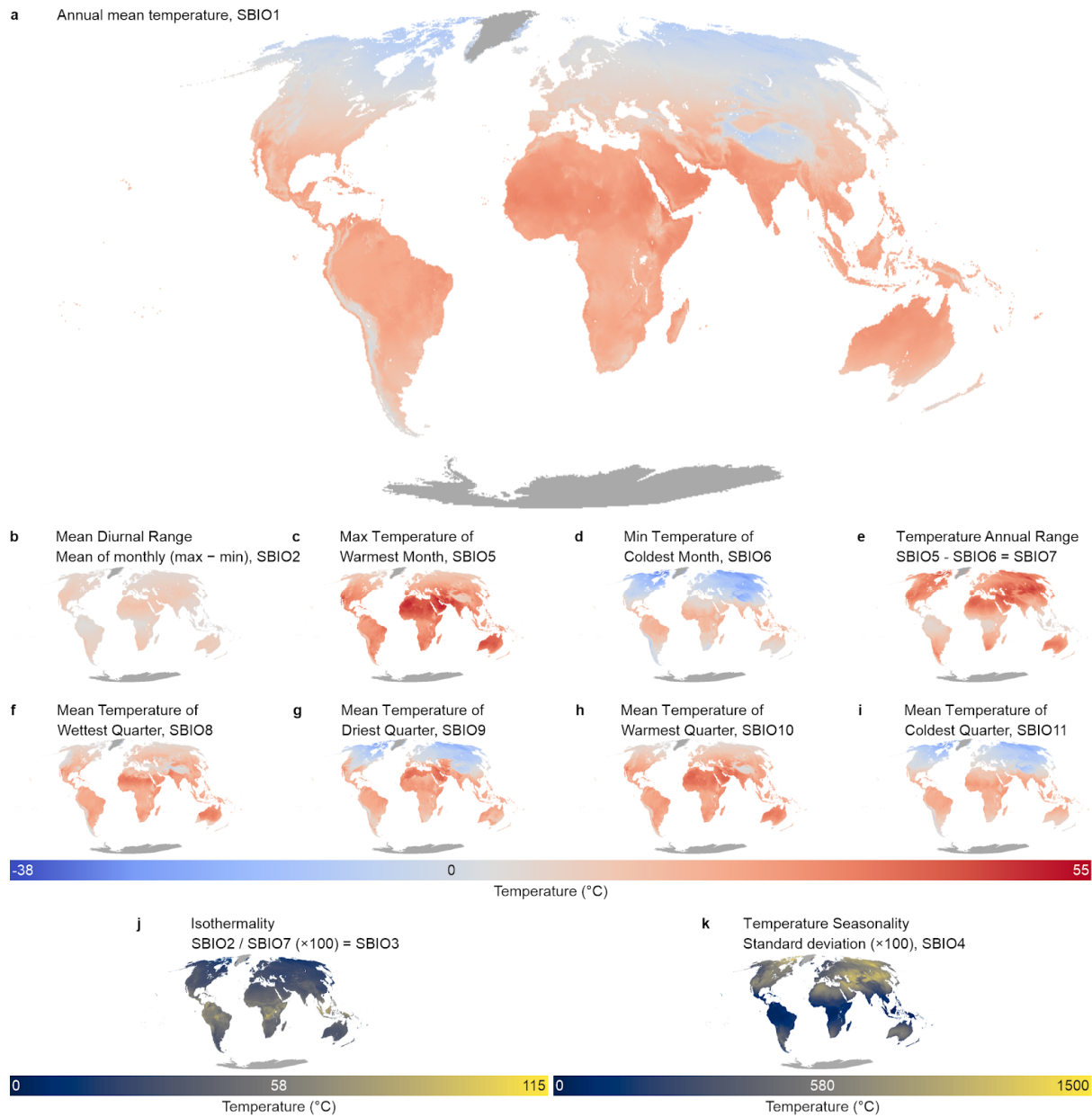
1468 biome (adapted from Whittaker 1970, based on geographic location of sensors averaged at 1 km²; 0–
1469 5 cm depth), ordered by mean temperature offset and coloured by mean annual precipitation. (c–d)
1470 Distribution of sensors in 2D climate space for the topsoil (c, 0–5 cm depth, N = 4530) and the second
1471 layer (d, 5–15 cm depth, N = 3989). Colours of hexagons indicate the number of sensors at each climatic
1472 location, with a 40 × 40 km resolution. Grey dots in the background represent the global variation in
1473 climatic space (obtained by sampling 1 000 000 random locations from the CHELSA world maps).
1474 Overlay with grey lines depicts a delineation of Whittaker biomes.

1475



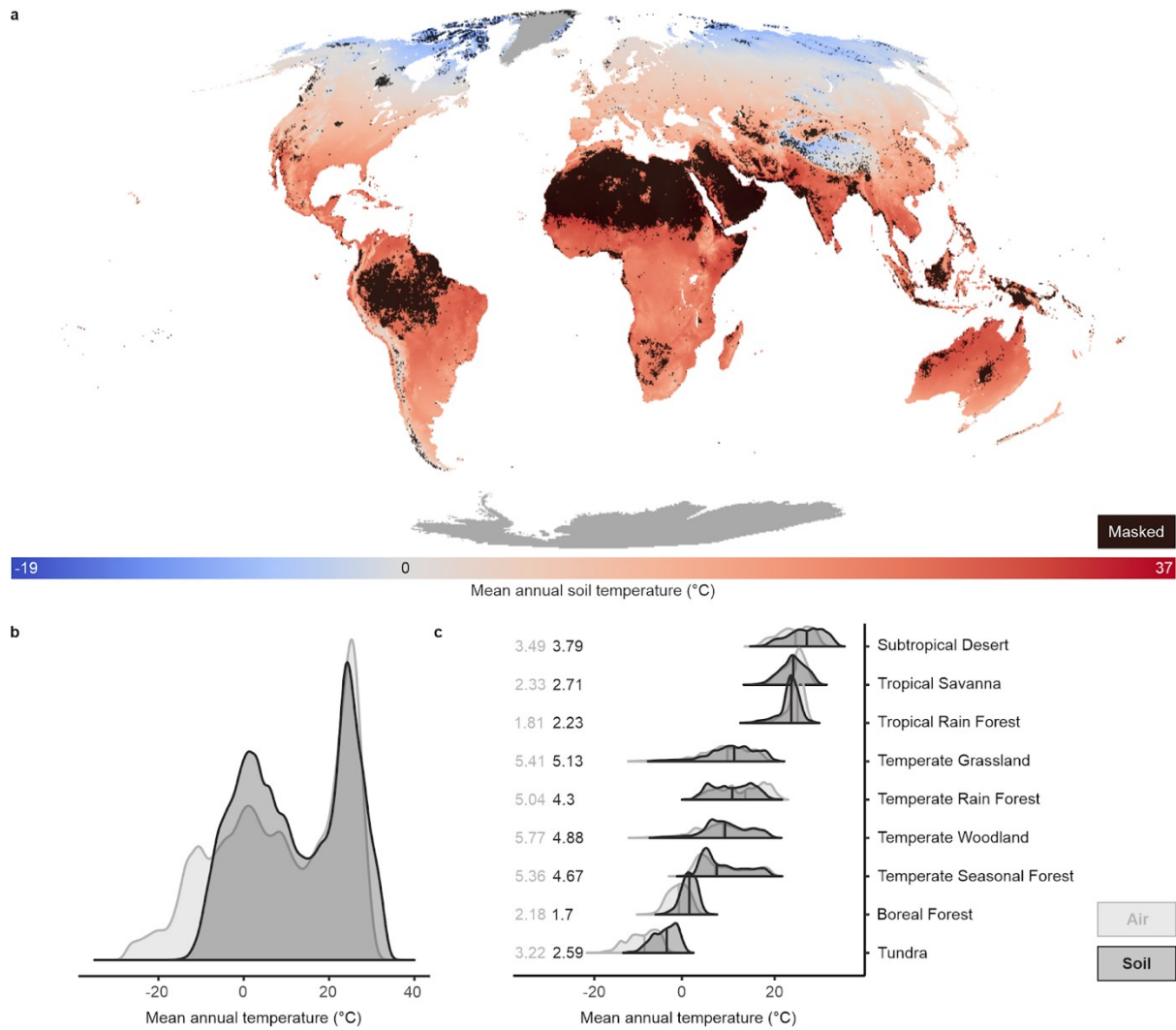
1476

1477 **Figure 2: Global modelled temperature offsets between soil and air temperature show strong**
 1478 **spatiotemporal variation across months.** Modelled annual (a) and monthly (b–m) temperature
 1479 **offset (in °C) between in situ measured soil temperature (topsoil, 0–5 cm) and gridded air**
 1480 **temperature. Positive (red) values indicate soils that are warmer than the air. Dark grey represents**
 1481 **regions outside the modelling area.**



1482 **Figure 3: Soil bioclimatic variables.** Global maps of bioclimatic variables for topsoil (0–5 cm depth)
 1483 climate, calculated using the maps of monthly soil climate (see Fig. 2), and the bioclimatic variables for
 1484 air temperature from CHELSA.
 1485

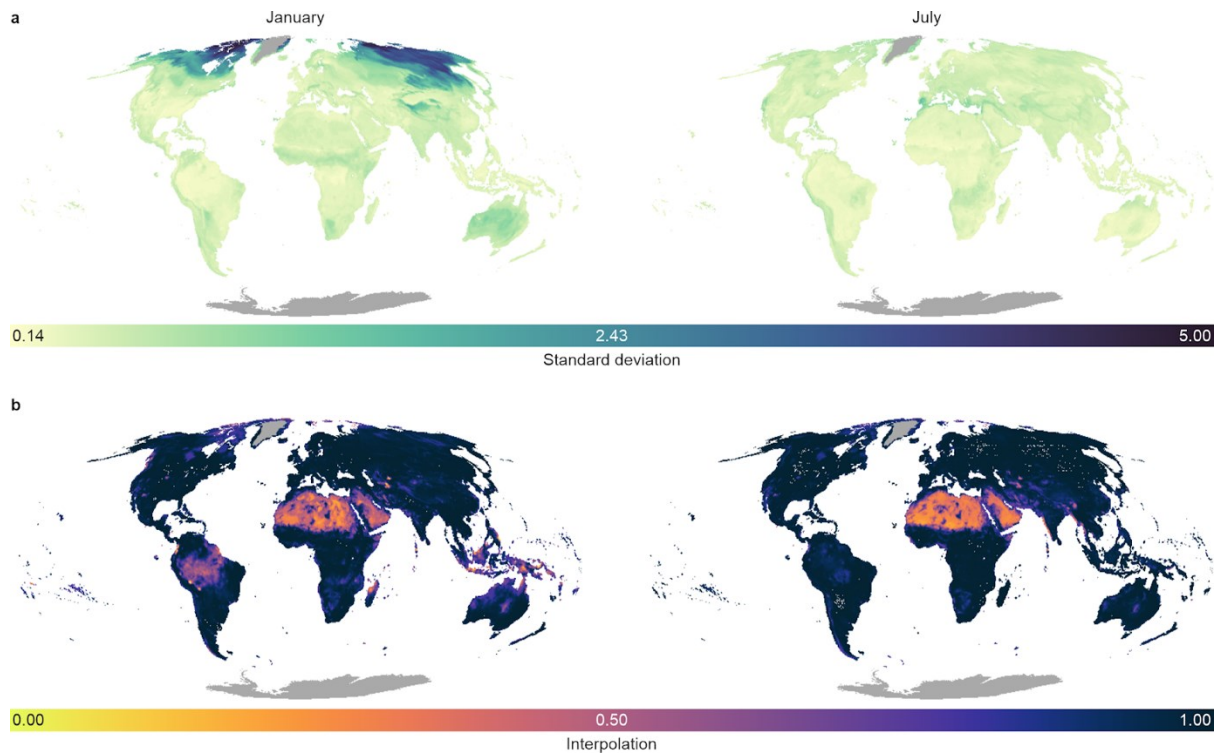
1486
1487



1488

1489 **Figure 4: Mean annual soil temperature shows significantly lower spatial variability than air**
 1490 **temperature.** (a) Global map of mean annual topsoil temperature (SBIO1, 0–5 cm depth, in $^{\circ}\text{C}$), created
 1491 by adding the monthly offset between soil and air temperature for the period 2000–2020 (Fig. 2) to
 1492 the monthly air temperature from CHELSA. A black mask is used to exclude regions where our models
 1493 are extrapolating (i.e., interpolation values in Fig. 5 are < 0.9 , 18% of pixels). Dark grey represents
 1494 regions outside the modelling area. (b–c) Density plots of mean annual soil temperature across the
 1495 globe (b) and for each Whittaker biome separately (c) for SBIO1 (dark grey, soil temperature),
 1496 compared with BIO1 from CHELSA (light grey, air temperature), created by extracting 1 000 000
 1497 random points from the 1-km 2 gridded bioclimatic products. The numbers in (c) represent the standard
 1498 deviations of air temperature (light grey) and soil temperature (dark grey). Biomes are ordered
 1499 according to the median annual soil temperature values from the highest temperature (subtropical
 1500 desert) to the lowest (tundra).

1501



1502

1503 **Figure 5: Models of the temperature offset between soil and air temperature have low standard**
 1504 **deviations and good global coverage.** Analyses for the temperature offset between in situ measured
 1505 topsoil (0–5 cm depth) temperature and gridded air temperature. (a) Standard deviation (in °C) over
 1506 the predictions from a cross-validation analysis that iteratively varied the set of covariates
 1507 (explanatory data layers) and model hyperparameters across 100 models and evaluated model
 1508 strength using 10-fold cross-validation, for January (left) and July (right), as examples of the two most
 1509 contrasting months. (b) The fraction of axes in the multidimensional environmental space for which
 1510 the pixel lies inside the range of data covered by the sensors in the database. Low values indicate
 1511 increased extrapolation.

1512

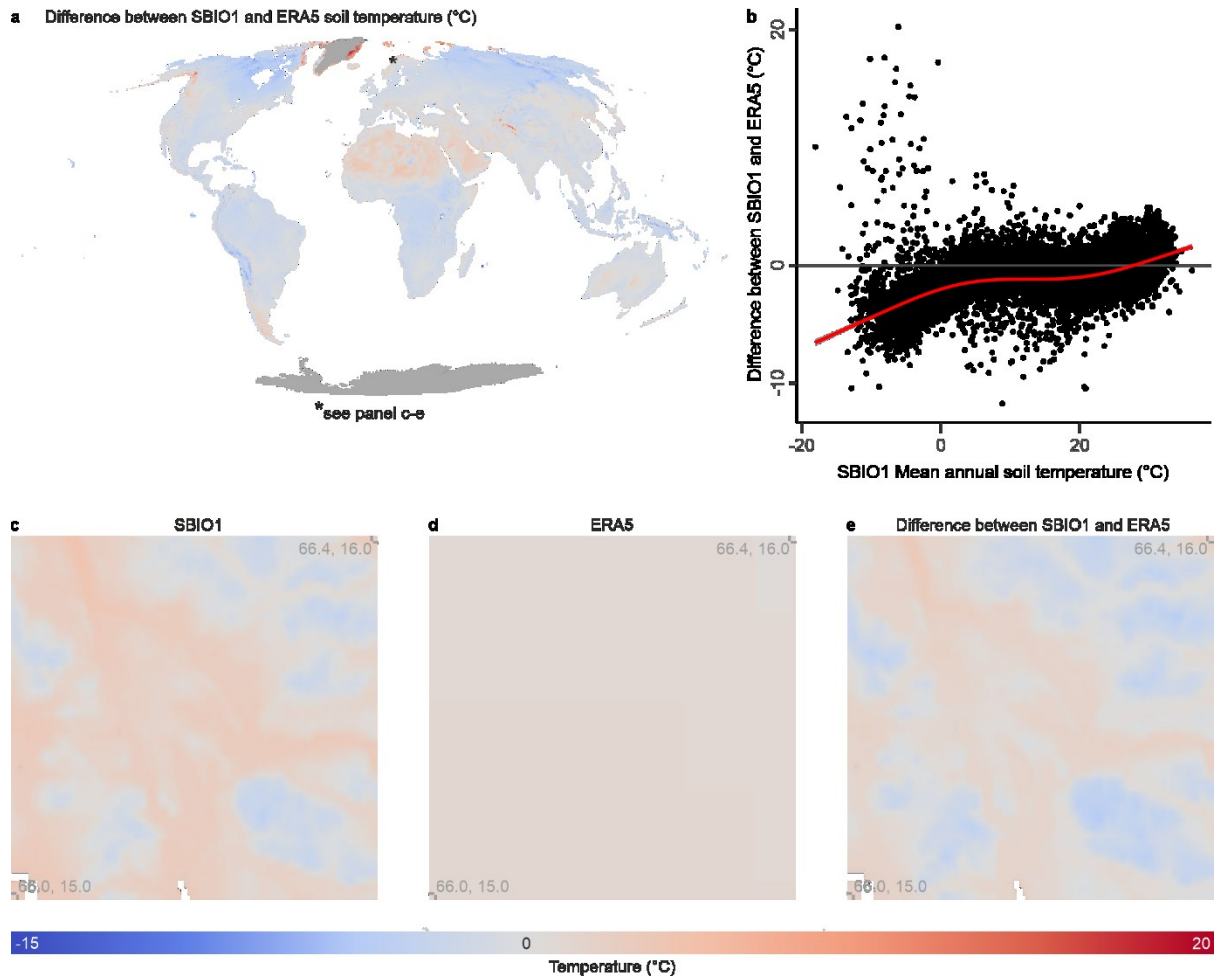


Figure 6: The mean annual soil temperature (SBIO1, 1 x 1 km resolution) modelled here is consistently cooler than ERA5L (9 x 9 km) soil temperature in forested areas. (a) Spatial representation of the difference between SBIO1 based on our model and based on ERA5L soil temperature data. Negative values (blue colours) indicate areas where our model predicts cooler soil temperature. Dark grey areas (Greenland and Antarctica) are excluded from our models. Asterisk in Scandinavia indicates the highlighted area in panels d to f (see below). (b) Distribution of the difference between SBIO1 and ERA5L along the macroclimatic gradient (represented by SBIO1 itself) based on a random subsample of 50 000 points from the map in a). Red line from a Generalized Additive Model (GAM) with $k=4$. (c-e) High-resolution zoomed panels of an area of high elevational contrast in Norway (from 66.0-66.4° N, 15.0-16.0° E) visualizing SBIO1 (c), ERA5L (d) and their difference (e), to highlight the higher spatial resolution as obtained with SBIO1.